Trafficking of K63-polyubiquitin–modified membrane proteins in a macroautophagy-independent pathway is linked to ATG9A

Francesco Scavone[a,†,*], Sharon Lian[a], Eeva-Liisa Eskelinen[b,c], Robert E. Cohen[a,*], and Tingting Yao[a,*]

[a]Department of Biochemistry and Molecular Biology, Colorado State University, Fort Collins, CO 80523, USA; [b]Molecular and Integrative Biosciences Research Programme, University of Helsinki, Helsinki, 00014, Finland; [c]Institute of Biomedicine, University of Turku, Turku, FI-20520, Finland

ABSTRACT **Cytoplasmic K63-linked polyubiquitin signals have well-established roles in endocytosis and selective autophagy. However, how these signals help to direct different cargos to different intracellular trafficking routes is unclear. Here we report that, when the K63-polyubiquitin signal is blocked by intracellular expression of a high-affinity sensor (named Vx3), many proteins originating from the plasma membrane are found trapped in clusters of small vesicles that colocalize with ATG9A, a transmembrane protein that plays an essential role in autophagy. Importantly, whereas ATG9A is required for cluster formation, other core autophagy machinery as well as selective autophagy cargo receptors are not required. Although the cargos are sequestered in the vesicular clusters in an ATG9-dependent manner, additional signals are needed to induce LC3 conjugation. Upon removal of the Vx3 block, K63-polyubiquitylated cargos are rapidly delivered to lysosomes. These observations suggest that ATG9A plays an unexpected role in the trafficking of K63-polyubiquitin–modified membrane proteins.**

SIGNIFICANCE STATEMENT

- K63-polyubiquitin acts as a signal for directing cargo to lysosomes via endocytosis or autophagy. However, how K63-polyubiquitylated proteins are sorted between these pathways remains unclear.
- By employing a sensor for cellular K63-polyubiquitin signals, the authors found that membrane proteins modified by K63-polyubiquitin can traffic to lysosomes via an ATG9A-associated vesicular pathway independent of other autophagic components.
- These findings support a role for K63-polyubiquitin and ATG9A in regulating membrane trafficking at the intersection between recycling and degradation.

Monitoring Editor
James Olzmann
University of California, Berkeley

Received: Dec 9, 2024
Revised: Feb 3, 2025
Accepted: Feb 5, 2025

This article was published online ahead of print in MBoC in Press (http://www.molbiolcell.org/cgi/doi/10.1091/mbc.E24-12-0535) on February 19, 2025.

[†]Present address: Department of Biology, Stanford University; Stanford, CA 94305, USA.

INTRODUCTION

Ubiquitin (Ub) can be conjugated to other proteins either as single ubiquitin(s) or as a polyubiquitin chain(s) (Pickart, 2001; Komander and Rape, 2012) assembled with various arrangements of ubiquitin–ubiquitin linkages (Peng *et al.*, 2003; Xu *et al.*, 2009). The prevailing model for a code determined by polyubiquitin linkage-type maintains that different types of polyubiquitin can signal functionally distinct outcomes via selective recognition by effector proteins that carry at least one ubiquitin-binding domain (UBD) (Pickart and Fushman, 2004; Husnjak and Dikic, 2012). K63-linked polyubiquitin (K63-polyUb), which does not target proteins for proteasomal degradation (Nathan *et al.*, 2013), serves as a signal to internalize transmembrane proteins at the plasma membrane such as the epidermal growth factor receptor (EGFR) and sort them into the intraluminal vesicles of multivesicular bodies (MVB) (Duncan *et al.*, 2006; Lauwers *et al.*, 2009; Huang *et al.*, 2013; Tsuchiya *et al.*, 2018). Canonical endolysosomal degradation requires maturation from early endosome to MVB followed by fusion with highly acidic, degradative lysosomes (Huotari and Helenius, 2011). The endosomal sorting complexes required for transport (ESCRT) contain UBDs that recognize ubiquitylated cargos in the endosomal membrane and sort them into intraluminal vesicles of MVBs, which are degraded in lysosomes (Raiborg and Stenmark, 2009; Shields and Piper, 2011; Piper *et al.*, 2014).

In addition to an established role for K63-polyUb in the turnover of endocytosed cargo, there is evidence that macroautophagy (henceforth referred to as "autophagy"), a pathway that extensively interconnects with endocytosis, may also use the K63-polyUb signal (Erpapazoglou *et al.*, 2014; Dósa and Csizmadia, 2022; Saeed *et al.*, 2023). In autophagy, intracellular material to be degraded is sequestered in double-membrane vesicles called autophagosomes and then released into lysosomes for their breakdown (He and Klionsky, 2009). ATG9A, a highly conserved transmembrane protein that is part of the core autophagy machinery, plays essential roles in autophagosome formation (Holzer *et al.*, 2024). Under basal conditions, ATG9A constitutively traffics to and from the plasma membrane, recycling endosomes, and the Golgi apparatus (Young *et al.*, 2006; Orsi *et al.*, 2012; Puri *et al.*, 2013). Upon autophagy induction (e.g., nutrient starvation), ATG9A vesicles relocalize to structures at the cell periphery corresponding to the sites of autophagy where they seed membrane from which the autophagosome grows (Maeda *et al.*, 2020; Matoba *et al.*, 2020; Sawa-Makarska *et al.*, 2020; Broadbent *et al.*, 2023; Olivas *et al.*, 2023). Recent studies have demonstrated that ATG9A exhibits lipid scramblase activity, which is thought to remodel membrane composition and induce membrane curvature during autophagosome expansion (Maeda *et al.*, 2020; Matoba *et al.*, 2020; Sawa-Makarska *et al.*, 2020; Broadbent *et al.*, 2023; Olivas *et al.*, 2023). Substantial evidence indicates a role for (poly)ubiquitin during selective autophagy, as several autophagic cargo receptors (e.g., p62/SQSTM1, Optineurin/OPTN, NDP52, NBR1, and TAX1BP1) sequester ubiquitylated substrates inside the growing autophagosome by simultaneous interactions with ubiquitin and LC3 (Johansen and Lamark, 2011; Adriaenssens *et al.*, 2022). Cargos such as misfolded proteins, toxic aggregates, and intracellular bacteria are marked by (poly)ubiquitin modification and engulfed by autophagosomes, which then fuse with late endosomes or lysosomal compartments. Previous studies have reported that K63-polyUb marks protein aggregates for their autophagic clearance (Tan *et al.*, 2008). Furthermore, K63-polyUb has been reported to modify host cellular proteins in endosomes that contain *Salmonella enterica* serovar Typhimurium as a response to membrane rupture (van Wijk *et al.* 2012; Fujita *et al.*, 2013). Analogous to endosomal damage, K63-polyUb also decorates dysfunctional lysosomes in response to membrane damage induced by exposure to L-Leucyl-L-Leucine methyl ester (LLOMe) (Papadopoulos *et al.*, 2017; Koerver *et al.*, 2019), possibly to recruit ESCRT or autophagic machineries for either repair or removal of membrane remnants (Hung *et al.*, 2013; Radulovic *et al.*, 2018; Skowyra *et al.*, 2018; Jia *et al.*, 2020; Eapen *et al.*, 2021).

Autophagy and endocytosis share some of the same machinery, such as the ESCRTs (Rusten and Stenmark, 2009; Lefebvre *et al.*, 2018). Depletion of individual ESCRT complexes in mammalian cells results in accumulation of autophagosomes (Filimonenko *et al.*, 2007; Lee *et al.*, 2007), likely as a consequence of inhibited fusion with the endolysosomal system (Tamai *et al.*, 2007) or defective autophagosomal membrane closure (Zhou *et al.*, 2019; Puri *et al.*, 2023). ESCRTs have also been implicated in alternative forms of autophagy (Sakai and Oku, 2024), including lysosomal microautophagy (Kuchitsu and Taguchi, 2024); here, lysosomes have been observed to engulf vesicles containing the transmembrane protein STING in an ESCRT and K63-polyUb–dependent manner to degrade STING and terminate STING signaling (Gentili *et al.*, 2023; Kuchitsu *et al.*, 2023).

Given the multifunctional roles of K63-polyUb in membrane protein trafficking and quality control in the endolysosomal system (Erpapazoglou *et al.*, 2014), we sought to better understand K63-polyUb function in endocytosis and autophagy, two distinct yet interconnected intracellular trafficking pathways. Questions remain in part due to the difficulty in monitoring K63-polyUb–dependent signaling within living cells. We have previously described a K63-polyUb–specific sensor, "Vx3," that can be used to detect and also to inhibit K63-polyUb–dependent signaling in cells (Sims *et al.*, 2012). Vx3 contains three ubiquitin interacting motifs (UIMs) connected by two 7-amino acid linkers designed to promote avid interaction with three adjacent ubiquitin moieties in K63-polyUb. Expression of Vx3-EGFP in living cells allows visualization and identification of cellular compartments enriched in K63-polyUb. Here we report our findings that K63-polyUb modifies a variety of plasma membrane proteins that are continually endocytosed and recycled to the cell surface. Surprisingly, Vx3 expression promotes accumulation of both K63-polyubiquitylated cargos and ATG9A into cytosolic clusters of small vesicles adjacent to late endosomes and lysosomes. By tightly binding to K63-polyUb, Vx3 inhibits receptors or deubiquitylating enzymes (DUBs) for K63-polyUb that may play important roles in promoting fusion of ubiquitylated cargo-containing vesicles with lysosomes. Our work supports a role for K63-polyUb in regulating lysosomal targeting of

Author contributions: F.S., R.E.C., and T.Y. conceived and designed the experiments; F.S., S.L., E.-L.E., R.E.C., and T.Y. performed the experiments; F.S., S.L., E.-L.E., R.E.C., and T.Y. analyzed the data; F.S., R.E.C., and T.Y. drafted the article; F.S. and E.-L.E. prepared the digital images.

Conflicts of interest: The authors declare no competing financial interests.

*Address correspondence to: Francesco Scavone (scavone@stanford.edu); Robert E. Cohen (Bob.Cohen@colostate.edu); and Tingting Yao (Tingting.Yao@colostate.edu).

Abbreviations used: DUB, deubiquitylase or deubiquitination enzyme; K63-polyUb, K63-linked polyubiquitin; USP2-cc, USP2 catalytic core; VMP1, Vacuole membrane protein 1.

membrane proteins via a vesicular trafficking pathway dependent on ATG9A but not other core autophagic machinery.

RESULTS

Vx3-EGFP is a sensor and inhibitor of selective autophagy pathways

We have previously reported that Vx3 tightly and selectively binds to K63-polyUb having three or more ubiquitins in the chain (Sims *et al.*, 2012). To study signaling by K63-polyubiquitin in vivo, we generated HeLa cells stably expressing Vx3 fused to EGFP under the control of a doxycycline (Dox)-inducible promoter (hereafter referred to as HeLa-Vx3^{SE} cells). Upon induction, Vx3-EGFP generates cytoplasmic foci that stain for K63-polyUb (Figure 1A) whereas a control protein ("Vx3NB") unable to bind polyubiquitin remains diffuse (Figure EV1A), indicating that Vx3 localization in these foci depends on its affinity for K63-polyUb. In the cytosol, K63-polyUb inclusions have been previously described as sites of autophagic clearance where polyubiquitin is used to recruit autophagy cargo receptors (Bjørkøy *et al.*, 2005; Pankiv *et al.*, 2007; Wooten *et al.*, 2008; Kirkin, McEwan *et al.*, 2009). We therefore examined the identity of the Vx3 foci by staining with a variety of autophagic and membrane protein markers (see Supplemental Dataset S1 for a summary of colocalization results). Strikingly, we found that Vx3 foci showed nearly complete colocalization with endogenous ATG9A (Figure 1B) but not components of the ULK1–kinase complex (ULK1 or FIP200) or other early autophagy regulators (ATG16L1 or WIPI2b) (Figure EV1, B–E). We also detected the autophagy cargo receptor p62/SQSTM1 localizing in the Vx3 foci (Figure EV1F), consistent with previous reports that p62/SQSTM1 preferentially interacts with K63-polyUb (Seibenhener *et al.*, 2004; Babu *et al.*, 2005; Wooten *et al.*, 2008; Wurzer *et al.*, 2015; Zaffagnini *et al.*, 2018). However, these Vx3 foci lacked detectable LC3 staining in the absence of autophagy induction ("No Treatment" in Figure 1C; Supplemental Dataset S1). Colocalization between Vx3 and LC3 was induced in response to stimuli known to activate selective autophagy such as bacterial infection, lipid-mediated transfection (Figure 1, C and D), or protein aggregation (Figure 2A). Importantly, LC3 was not observed in Vx3 foci when cells were subject to nutrient starvation (Figure 1C), despite that abundant LC3 foci were observed under this condition. In contrast, we found that ~55% of Vx3 foci colocalized with endogenous LC3 when Vx3-EGFP was introduced into wild-type (WT) HeLa cells by transient transfection with the cationic lipid Lipofectamine (hereafter indicated as Vx3^{TT}; TT = *Transient Transfection*) (Figure 1D). Treatment with Lipofectamine, even without DNA, induced Vx3 signals in puncta that colocalized with LC3 (Figure 1C). Treatments with other lipid-based reagents such as Effectene yielded similar results (Figure EV1G). Punctate Vx3 and LC3 signals also overlapped with ATG9A (Figure EV1H). These LC3-positive structures were decorated with galectin-3 (Figure EV1I), a marker of damaged membranes, suggesting that they are sites of selective autophagy associated with endomembrane rupture (Fujita *et al.*, 2013). Similarly, when Dox-induced HeLa-Vx3^{SE} cells were infected with *S. enterica* serovar Typhimurium, Vx3 surrounded a subpopulation of intracellular *Salmonella* that associated with LC3 (Figure 1C) and galectin-3 (Figure EV1I).

As Vx3 displays higher affinity than any of the known naturally-occurring receptors for K63-polyUb, it is likely to compete for endogenous K63-polyUb–dependent interactions within living cells, thereby interfering with selective autophagy signaling (Sims *et al.*, 2012). To test this, HEK293 cells expressing Dox-inducible Vx3 or Vx3NB were infected with *Salmonella* and intracellular bacterial growth was monitored. Intracellular proliferation of *Salmonella* was significantly higher in the presence of Vx3 (Figure 1E), indicating that Vx3 expression inhibited selective autophagy of the *Salmonella*. In contrast, the increase in LC3 puncta observed upon starvation was not affected by Vx3 expression (Figure 1F). Together, these findings indicate that K63-polyUb is not required for nonselective autophagy that is observed upon nutrient starvation. Vx3 localizes and inhibits signaling at selective autophagy sites induced by membrane damage. Notably, Vx3 also colocalized with ATG9A in distinct structures that are not conventional autophagic sites.

Vx3-EGFP foci are clusters of vesicles containing ATG9A and K63-polyubiquitin

Previous reports showed that expression of the multispanning membrane protein VMP1 fused to fluorescent protein tags stimulates autophagy by generating cytoplasmic foci that stain for ubiquitin (Ropolo *et al.*, 2007; Karanasios *et al.*, 2016; Renna *et al.*, 2023). During the process of screening for autophagic markers that colocalize with Vx3 foci, we found that expression of VMP1-iRFP induced the appearance of LC3 at Vx3 foci in HeLa-Vx3^{SE} cells (Figure 2A); this result is similar to those from the endomembrane rupture treatments. Stable coexpression of VMP1-iRFP and Vx3 in the absence of Lipofectamine treatment induced Vx3 foci that showed a high degree of colocalization with multiple autophagy markers that included LC3, ATG9A, p62/SQSTM1, and NBR1 (Figure 2, A–C; Figure EV2A; Supplemental Dataset S1), suggesting that they represent sites of selective autophagy. However, endogenous VMP1 does not form the punctate structures but colocalizes with markers of the ER (Zhao *et al.*, 2017). We found that Vx3-EGFP co-immunoprecipitated (co-IP) polyubiquitylated VMP1-iRFP but not endogenous VMP1 (Figure 2D). Thus, either overexpression of VMP1 or the fusion of a fluorescent protein tag to the C-terminus of VMP1 most likely promoted its aggregation, K63-polyubiquitylation (Figure EV2B) and selective autophagy (Figure 2, A–C; Figure EV2A). These results are consistent with earlier reports of VMP1-GFP aggregation and autophagy induction upon its overexpression (Ropolo *et al.*, 2007; Itakura and Mizushima, 2010; Karanasios *et al.*, 2016; Zhao *et al.*, 2017; Renna *et al.*, 2023). We therefore used the HeLa cell line made to stably express both Vx3 and VMP1-iRFP (hereafter called HeLa-Vx3^{SE}-VMP1) as a model system to produce abundant large Vx3 foci, likely as a consequence of VMP1-iRFP aggregation (compare panels in Figure 2 and Figure 1).

To investigate the nature of the Vx3–ATG9A–VMP1-containing foci, we performed correlative light-electron microscopy (CLEM) with HeLa-Vx3^{SE}-VMP1 cells transiently transfected with mCherry-ATG9A. Structures containing EGFP, mCherry, and iRFP were first identified and imaged by fluorescence confocal microscopy with Airyscan enhanced resolution and then analyzed by transmission electron microscopy (TEM) (Figure 2E). We found that the Vx3 foci corresponded to heterogeneous clusters of small, tightly-packed and mostly single-membrane vesicles exhibiting different electron densities and sizes (50–150 nm diameter) (Figure 2E), suggesting that they were blocked in their fusion or trafficking. In the TEM images of 100-nm sections, the Vx3-containing foci appeared heterogeneous; some contained small double-membrane vesicles or tubules (see Figure 2F, *panel II*) whereas in other cases small single-membrane vesicles were found within larger double-membrane structures (see Figure 2F, *panel I*). Airyscan confocal

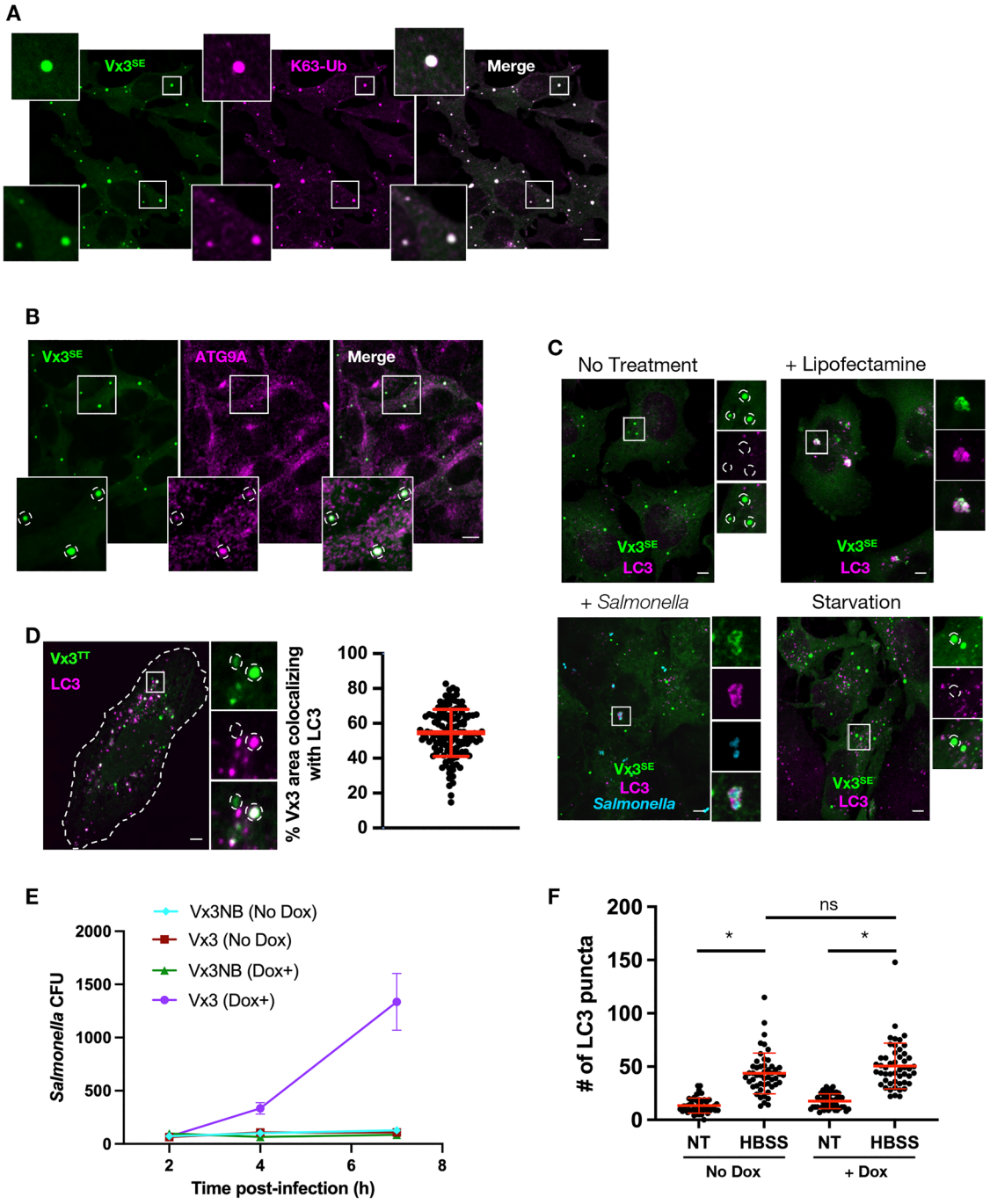

FIGURE 1: Vx3 is a sensor and an inhibitor of selective autophagy pathways. (A) Vx3-EGFP (Vx3) localizes in cytoplasmic foci that contain K63-polyUb. Maximum projection image of HeLa-Vx3^{SE} (*green*) cells fixed 24 h after induction with Dox and stained with anti-Ub K63-specific monoclonal antibody (*magenta*). Representative magnified images of the boxed areas show colocalization of Vx3 foci with K63-polyUb. Scale bar: 10 μm. (B) Vx3-EGFP colocalizes with endogenous ATG9A. Vx3 is *green*. The cells were immunostained with anti-ATG9A (*magenta*). Inset panels show positions of Vx3 foci marked with dotted circles. Scale bar: 10 μm. (C) Induction of selective autophagy promotes Vx3-EGFP and LC3 colocalization. HeLa-Vx3^{SE} cells were treated with Dox for 24 h before either addition of Lipofectamine for 4 h, infection with *Salmonella* for 1 h, or nutrient starvation with HBSS (*Starvation*) for 1 h. Cells were stained with anti-LC3 (*magenta*). Zoomed panels from Lipofectamine treatment or *Salmonella* infection (*light blue*) show overlap between Vx3 (*green*) and endogenous LC3; no overlap is observed in untreated or nutrient-starved HeLa cells expressing Vx3 (see *white* dotted outlines of Vx3 foci projected onto the LC3 channel). Scale bars: 5 μm. (D) Transiently transfected Vx3-EGFP forms foci that colocalize with LC3. *Left panel*: HeLa cells transiently transfected with Vx3^{TT} (*green*) for 24 h and stained with anti-LC3 antibody (*magenta*); dashed line shows cell boundary. Magnified images of the boxed area show selected Vx3 foci (*white* dotted circles). *Right panel*: Analysis from >100 cells showed that 54% of Vx3^{TT} foci colocalized with LC3. Scale bar: 5 μm. (E) Vx3 expression inhibits selective autophagy of *Salmonella*. HEK293-Vx3NB and HEK293-Vx3 cells, untreated or treated with Dox for 48 h, were infected with RFP-containing

images showed that mCherry-ATG9A was adjacent to and only partially overlapped with Vx3 (Figures 2, E and G and EV2C), indicating that ATG9A-positive subdomains are distinct from the Vx3-bound structures. On the other hand, the Vx3 and VMP1-iRFP signals were largely coincident (Figures 2G and EV2C), supporting the idea that vesicles with VMP1-iRFP contain K63-polyUb that are distinct from those containing ATG9A.

Vx3-EGFP expression causes accumulation of K63-polyubiquitylated cargo of plasma membrane origin in close proximity to endolysosomes

To identify endogenous proteins modified with K63-polyUb and bound by Vx3-EGFP, we immunoprecipitated Vx3 using GFP-Trap resin followed by LC-MS/MS analysis. The high affinity between Vx3 and K63-polyUb (Sims *et al.*, 2012) allowed us to do pull-downs of Vx3 under stringent, semidenaturing conditions (see *Materials and Methods*). We performed this protocol with lysates from three stable cell lines: HeLa cells expressing Vx3NB as a control, HeLa-Vx3^{SE} cells, and, to determine whether additional proteins associate with Vx3-EGFP upon VMP1-iRFP overexpression, HeLa-Vx3^{SE}-VMP1 cells. Results of the proteomics analyses showed that the most prominent hits were proteins known to localize at the plasma membrane (Supplemental Dataset S2); these included transferrin receptor (TfR), MHC class I HLA-A (MHC-I), and caveolin-1 (CAV-1). Overexpression of VMP1-iRFP led to identification of additional proteins associated with Vx3-EGFP, the majority of which are also membrane proteins (Supplemental Dataset S2). This result is consistent with the increased number of cytosolic Vx3 foci observed upon VMP1-iRFP overexpression (compare panels in Figure 2 and Figure 1). Notably, peptides from VMP1 were identified only in immunoprecipitates from the VMP1-iRFP expressing cells (Supplemental Dataset S2), consistent with our earlier analyses that the tagged and overexpressed VMP1 but not endogenous VMP1 is modified by K63-polyUb and bound by Vx3 (Figure 2D). The autophagic adaptor p62/SQSTM1 was also immunoprecipitated by Vx3, in agreement with our colocalization data (Figures EV1F and 2C; Supplemental Dataset S1). In contrast, despite its extensive colocalization in the Vx3 foci, ATG9A was not found in the Vx3 pulldown (Supplemental Dataset S2). This observation supports the results from Airyscan confocal microscopy that showed Vx3 and ATG9A localized to distinct subdomains within the foci (Figure 2, E and G).

We confirmed some of the hits from the proteomic analyses using antibodies. Whereas the vast majority of endogenous TfR localized in small puncta in the perinuclear region and around the cytoplasm as previously reported (Raiborg *et al.*, 2002), we observed that a small fraction of TfR accumulated in Vx3 foci that were also positive for ATG9A, (Figure 3A; Supplemental Dataset S1). Similarly, subpopulations of MHC-I (Figure EV3A) and CAV-1 (Figure EV3B) colocalized with Vx3 foci. Endogenous TfR and MHC-I were also enriched in Vx3 foci that accumulated upon stable expression of VMP1-iRFP (Figures EV3C and EV3D). Given the stringent conditions used for the immunoprecipitations, we expected that many and perhaps most of the proteins identified by LC-MS/MS were modified directly by K63-polyUb. We therefore evaluated ubiquitylation status by treating Vx3 immunoprecipitants with purified recombinant DUBs. The Vx3 pulldown contained high molecular weight forms of TfR (Figure 3B). Upon treatment with AMSH, a K63 linkage-specific DUB (McCullough *et al.*, 2004) or USP2-cc, a linkage nonspecific DUB (Ryu *et al.*, 2006), the smear of high molecular weight forms of TfR was converted to a band corresponding to the ~85 kDa size of monomeric TfR expected after polyubiquitin removal. In contrast, treatment with OTUB1, a K48-linkage specific DUB (Edelmann *et al.*, 2009), had no effect (Figure 3B).

Mature TfR resides on the plasma membrane, but after endocytosis it typically traffics to recycling endosomes or Golgi and then returns to the cell surface (Ullrich *et al.*, 1996; Mayle *et al.*, 2012). Immunostaining for early endosome antigen 1 (EEA1) or Rab11a showed that Vx3 foci did not colocalize with markers of early or recycling endosomes, respectively (Figures EV3E and EV3F). Vx3 foci were also negative for the Golgi apparatus markers GM130 and TGN-38 (Figures EV3G and EV3H). Rather, ~80% of Vx3 foci colocalized with CD63 and Rab7a (Figure 3C; Supplemental Dataset S1) or LAMP1 (Figure 3D), markers of late endosomes and lysosomes. Airyscan confocal images showed that CD63 and Rab7a or LAMP1 signals did not have coincident staining patterns and partially overlapped with Vx3 (Figure 3, E and F), suggesting that like the ATG9A-containing vesicles, the structures positive for the late endosomal markers are distinct from vesicles that are decorated by K63-polyubiquitylated cargo. To visualize localization of Vx3-EGFP relative to the endolysosomal membrane, we took advantage of the abnormally large (1–5 μm diameter) endosomes that form upon overexpression of the GTPase-defective Rab5 mutant Rab5Q79L (Stenmark *et al.*, 1994). In HeLa WT cells transfected to express both Vx3^{TT} and mCherry-Rab5Q79L, Vx3-EGFP appeared to localize at a single site on the cytoplasmic side of the limiting membrane of the enlarged endolysosome (Figure 3G; Supplemental Video S1). Interestingly, coexpression of the BiP ER signal sequence fused to BFP together with the ER retrieval peptide KDEL (BFP-KDEL) (Friedman *et al.*, 2011) showed Vx3 foci contacting simultaneously both the endolysosome and a BFP-KDEL-positive ER tubule (Figure 3G; Supplemental Video S1). Immunostaining with ER markers SEC31a (Figure EV3I) and calnexin (CNX) (Figure EV3J) showed that Vx3 foci are distinct from but often close to the ER. Analogously, overexpression of mCherry-SEC61β (Figure EV3K) often showed ER tubules in contact with Vx3 foci.

When examined by immuno-EM, we found that the Vx3-containing membranes were clustered in proximity to but distinct from the enlarged Rab5Q79L endosomes (Figures 3H and EV3L). Anti-GFP immunogold particles were mostly seen at the cytoplasmic side of the Vx3-containing membranes (see zoomed panels I and II in Figure 3H and Figure EV3L), although in rare cases they were also detected on the edges of intraluminal vesicles that appear to be within multivesicular bodies (see Figure EV3M). Altogether, these data suggest that Vx3-EGFP traps K63-polyubiquitylated membrane proteins in close proximity to endolysosomes, likely blocking their delivery into degradative compartments.

Salmonella. Cells were lysed 2, 4, and 7 h postinfection, plated on selective agar plates, and bacterial colony-forming units (CFU) were counted; error bars indicate the SD from the mean of three experiments. (F) Vx3 expression does not perturb starvation-induced autophagy. HeLa-Vx3^{SE} cells untreated or treated with Dox for 24 h were cultured in DMEM containing 10% (vol/vol) FBS (NT) or HBSS for 1 h and stained for LC3; autophagosomes (i.e., LC3 dots) per cell were counted from 50 cells per condition. Error bars indicate the SD from the mean; unpaired two-tailed *t* test results were grouped as $p > 0.05$ (*ns*) and $p < 0.05$ (*asterisk*).

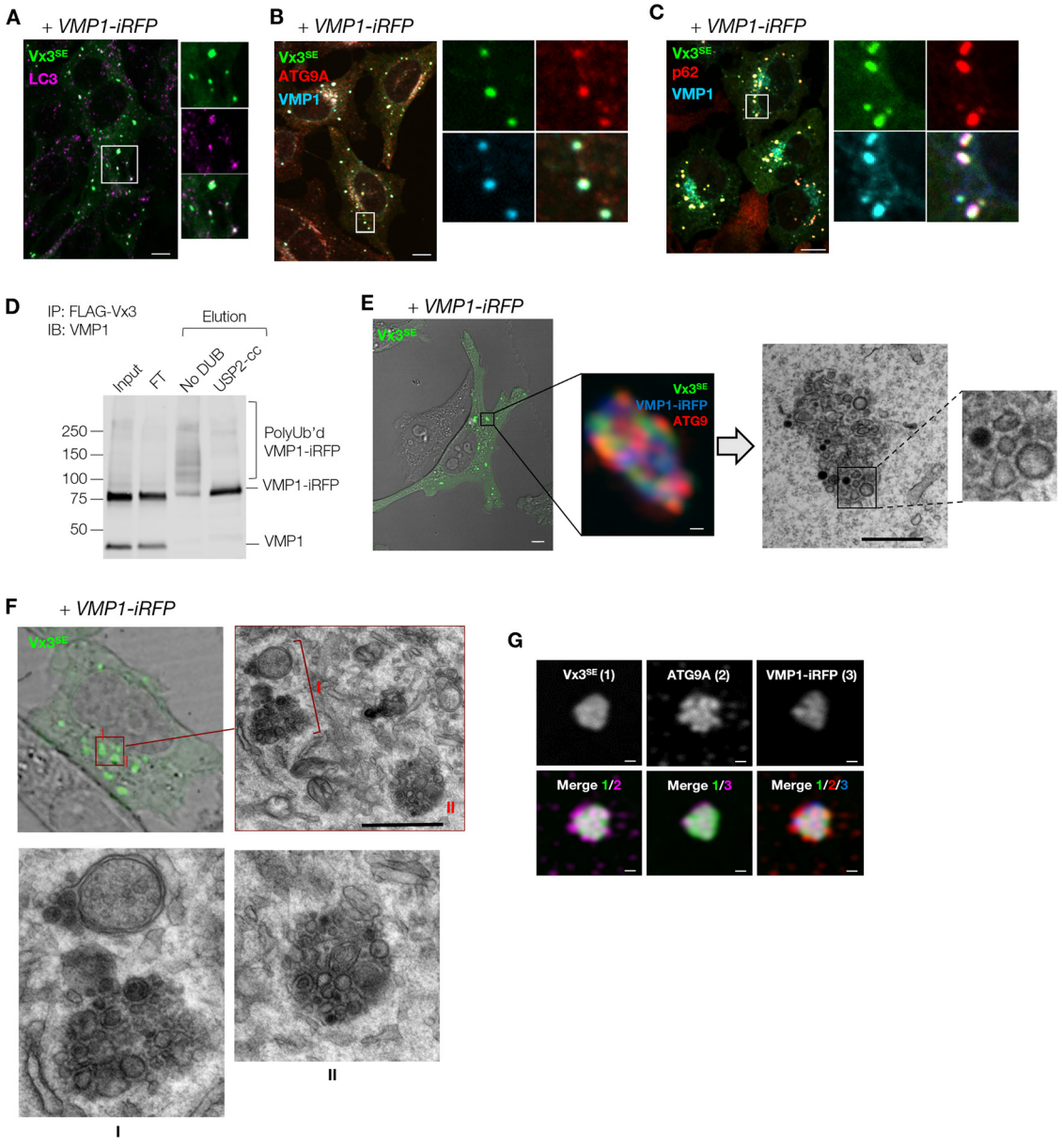

FIGURE 2: Vx3-EGFP foci are clusters of vesicles containing ATG9A and K63-polyUb. (A) Expression of VMP1-iRFP induces Vx3-EGFP and LC3 colocalization. HeLa-Vx3^{SE} cells were stably transduced with VMP1-iRFP and treated with Dox for 24 h; cells were stained with anti-LC3 antibody. Zoomed panels show overlap between Vx3 (*green*) and endogenous LC3 (*magenta*). Scale bar: 10 μm. (B) Vx3-EGFP colocalizes with VMP1-iRFP and ATG9A. HeLa-Vx3^{SE} cells prepared as in A were analyzed to visualize VMP1-iRFP (*light blue*), Vx3 (*green*), and stained with anti-ATG9A antibody (*red*). Magnified images of the boxed area illustrate colocalization of the three proteins. (C) Vx3-EGFP colocalizes with VMP1-iRFP and p62/SQSTM1. HeLa-Vx3^{SE} cells as in A were analyzed to visualize VMP1-iRFP (*light blue*), Vx3 (*green*), and stained with an anti-p62/SQSTM1 antibody (*red*). Magnified images of the boxed area illustrate colocalization of the three proteins. Scale bar: 10 μm. (D) VMP1-iRFP but not endogenous VMP1 is K63-polyubiquitylated. HeLa-Vx3^{SE}-VMP1 cells, stably coexpressing FLAG-tagged Vx3 and VMP1-iRFP, were treated with Dox for 48 h before subjecting whole-cell lysates to FLAG-Vx3 immunoprecipitation with anti-FLAG M2 agarose beads. The VMP1-immunoreactive smear in lane 3 ("No DUB") corresponds to polyubiquitylated VMP1. Proteins were directly digested with a pan-specific DUB (USP2-cc) while bound to the beads to deconjugate the polyUb chains from the substrate and detect the unmodified form of the protein. The anti-VMP1 antibody detects both endogenous VMP1 and VMP1-iRFP; FT, flowthrough. (E) CLEM shows that Vx3-EGFP foci comprise clusters of vesicles containing VMP1-iRFP and ATG9A. HeLa-Vx3^{SE}-VMP1 cells were transiently transfected with mCherry-ATG9A and treated with Dox for 24 h. The left panel is an overlay of phase contrast and Vx3 fluorescence (*green*) images. Foci containing Vx3, mCherry-ATG9A (*red*) and VMP1-iRFP (*blue*) were first imaged by fluorescence confocal microscopy with Airyscan superresolution (scale bar: 5 μm) and subsequently imaged in 100-nm thin sections by TEM (scale bar: 0.5 μm). (F) CLEM images reveal that HeLa-Vx3^{SE}-VMP1 cytoplasmic foci are comprised of heterogeneous membranous structures. The upper left panel is an overlay of phase contrast and Vx3 (*green*) images. Upper right panel: TEM of a 100-nm section

Vx3-EGFP expression inhibits delivery of K63-polyubiquitylated transmembrane protein cargo to endolysosomes

To investigate the relationship between Vx3 foci and active lysosomes, we used Lysotracker Red, which labels intracellular acidic compartments, and DQ-BSA Red, whose fluorescence indicates active proteolysis. Although Vx3 foci overlap with CD63 or Rab7a and LAMP1 (Figure 3, C–F), they are clearly distinct from structures stained by Lysotracker or DQ-BSA, indicating that they are not degradative compartments (Figure 4A). To elucidate the itinerary of K63-polyubiquitylated transmembrane protein cargo downstream of the Vx3 block, we took advantage of the destabilizing domain called "DD," a variant of FKBP12, fused to Vx3-EGFP (DD-Vx3-EGFP). Proteins expressed as fusions with DD are rapidly degraded by the proteasome but can be stabilized by Shield1, a reversibly-bound cell-permeable ligand (Banaszynski *et al.*, 2006). By using a combination of Dox and Shield1 to control both transcription and degradation of DD-Vx3-EGFP, we were able to control delivery and release of the Vx3-EGFP block in HeLa cells. After addition of Dox and Shield1 for 24 h, transiently transfected DD-Vx3-EGFP (hereafter indicated as DD-Vx3^{TT}) localized to cytosolic puncta similar to Vx3-EGFP either transiently or stably expressed (Figure 4B). At 10 h after removal of Dox and Shield1, most cell EGFP fluorescence had decreased to background levels (Figure 4B).

To monitor the fate of K63-polyubiquitylated transmembrane protein cargo upon its release from Vx3-EGFP, we needed to differentiate the cargo (e.g., K63-polyubiquitylated TfR) sequestered in Vx3 foci from the larger population (likely, not ubiquitylated) residing on recycling endosomes or the plasma membrane. To address this issue, we expressed TfR fused to HALO-Tag (TfR-HALO) and supplied the cells with PA-JF646, a cell-permeable and photoactivatable HALO-Tag ligand (Grimm *et al.*, 2016). The TfR-HALO proteins were then photoactivated selectively at DD-Vx3^{TT} foci (Figure EV4A) and monitored following Dox and Shield1 washout. Live-cell imaging revealed that the TfR-HALO in the foci disassembled into small fluorescent structures that moved away from the initial photoactivation site (Figure 4, C and D; Supplemental Video S2). Strikingly, photoactivated TfR-HALO that left the DD-Vx3^{TT} foci then colocalized with Lysotracker (Figure 4, C and D; Supplemental Video S2), indicating that the TfR-containing vesicles became associated with acidic lysosomes. The Lysotracker signal was often seen contacting and remaining associated with TfR-HALO for several minutes (up to 15 min) before disassociating along with a fraction of the TfR-HALO signal (Figure 4D). The transfer of photoactivated TfR to Lysotracker-positive structures occurred at the sites where Lysotracker contacted DD-Vx3^{TT} foci (Figure 4, A and C; Supplemental Video S2), suggesting that disassociation of TfR-containing vesicles from the Vx3-EGFP–induced cluster coincided with their fusion with the lysosome. To address the fate of ATG9A-containing vesicles within the Vx3 foci, we similarly cotransfected HALO-ATG9A and DD-Vx3^{TT}. In contrast to TfR-HALO, photoactivated HALO-ATG9A rapidly moved away from the DD-Vx3^{TT} foci and did not colocalize with Lysotracker (Figures EV4B and EV4C; Supplemental Video S3), indicating that ATG9A was not incorporated into lysosomes.

The results above suggest that Vx3 expression blocks delivery of K63-polyubiquitylated plasma membrane proteins into degradative lysosomes. Under normal conditions, the fate of this subpopulation of TfR is reminiscent of EGFR, which is endocytosed via clathrin-coated vesicles and whose modification by K63-polyUb leads to degradation by the ESCRT-dependent MVB pathway (Duncan *et al.*, 2006; Lauwers *et al.*, 2009; Huang *et al.*, 2013; Tsuchiya *et al.*, 2018). Vx3 foci colocalized with ligand-bound EGFR (Figure EV4D), supporting that K63-polyubiquitylated cargo of plasma membrane origin accumulates within Vx3-EGFP foci. Thus, we sought to determine whether disruption of the ESCRT function alters Vx3-EGFP distribution. We observed that overexpression of retroCHMP3, a fragment of CHMP3 that blocks assembly of functional ESCRT-III (Rheinemann *et al.*, 2021), dramatically increased the number of Vx3 foci (Figure 4E). Similarly, siRNA-mediated knockdown of USP8, a deubiquitinating enzyme that regulates endocytic cargo degradation through interaction with ESCRT-0 (Niendorf *et al.*, 2007), also promoted accumulation of Vx3 foci (Figure EV4E). Thus, the Vx3/ATG9 clusters may represent an alternative pathway to degrade K63-polyubiquitylated transmembrane proteins that otherwise would be trafficked through ESCRT-dependent pathway(s).

ATG9A but not other core autophagic components is required for Vx3-EGFP foci formation

Although we consistently observed a high degree of colocalization of ATG9A with Vx3 foci, the appearance of LC3 at those foci depended on additional autophagic stimuli (see panels in Figures 1 and 2). To determine whether Vx3-EGFP foci formation depends on the autophagic machinery, we used RNA-interference to reduce expression of several autophagy-related genes in HeLa-Vx3^{SE} (Supplemental Dataset S3). Strikingly, siRNA targeting ATG9A markedly decreased Vx3 foci (Figures 5A, EV5A, EV5B, and EV5C), whereas RNAi targeting VMP1 had no effect (Figure EV5C and EV5E); this is consistent with our previous observation that endogenous VMP1 is not associated with Vx3-EGFP foci (Figure 2D). Importantly, depletion of other early autophagy regulators, including ATG5 (Figures 5B and EV5D), FIP200 (Figure EV5D), ULK1, ATG14, Beclin1, and ATG16L1 (Figure EV5E) did not reduce the Vx3 signal (Supplemental Dataset S3). To directly test the dispensability of LC3 during Vx3 foci formation, we employed a previously described HeLa cell line (HeLa hATG8s-KO) lacking the six human ATG8 proteins (LC3A, LC3B, LC3C, GABARAP, GABARAPL1, GABARAPL2) (Nguyen *et al.*, 2016). Expression of DD-Vx3^{TT} in HeLa hATG8s-KO cells showed similar punctate distribution when compared with WT control (Figure EV5D). Altogether, these results suggest that proteins needed for autophagosome biogenesis are not required for Vx3 foci formation.

The marked decrease in Vx3 foci upon ATG9A depletion is not due to global reduction of intracellular K63-polyUb (Figure EV5F). Rather, a variety of perturbations to ATG9A trafficking consistently interfered with Vx3 foci formation (Supplemental Dataset

of areas with fluorescent Vx3 foci. Insets (I) and (II) show the presence of double membranes and clusters of vesicles that correspond to the Vx3−ATG9A−VMP1 foci identified by Vx3 fluorescence (*green*). Scale bar: 1 µm. (G) Airyscan superresolution images of Vx3-EGFP foci. Single z-section of a Vx3−ATG9A−VMP1 focus from a HeLa-Vx3^{SE}-VMP1 cell prepared as in A. Single-color images of each channel are shown in *white* (top row). Pairwise combinations between Vx3 (*green*) and ATG9 (*magenta*) or VMP1 (*magenta*) show that Vx3 and VMP1 exhibit a similar staining pattern while Vx3 and ATG9A patterns are different; a three-color merged image is also shown (bottom row: Vx3 (*green*), ATG9 (*red*), and VMP1 (*blue*)). Scale bars: 0.1 µm.

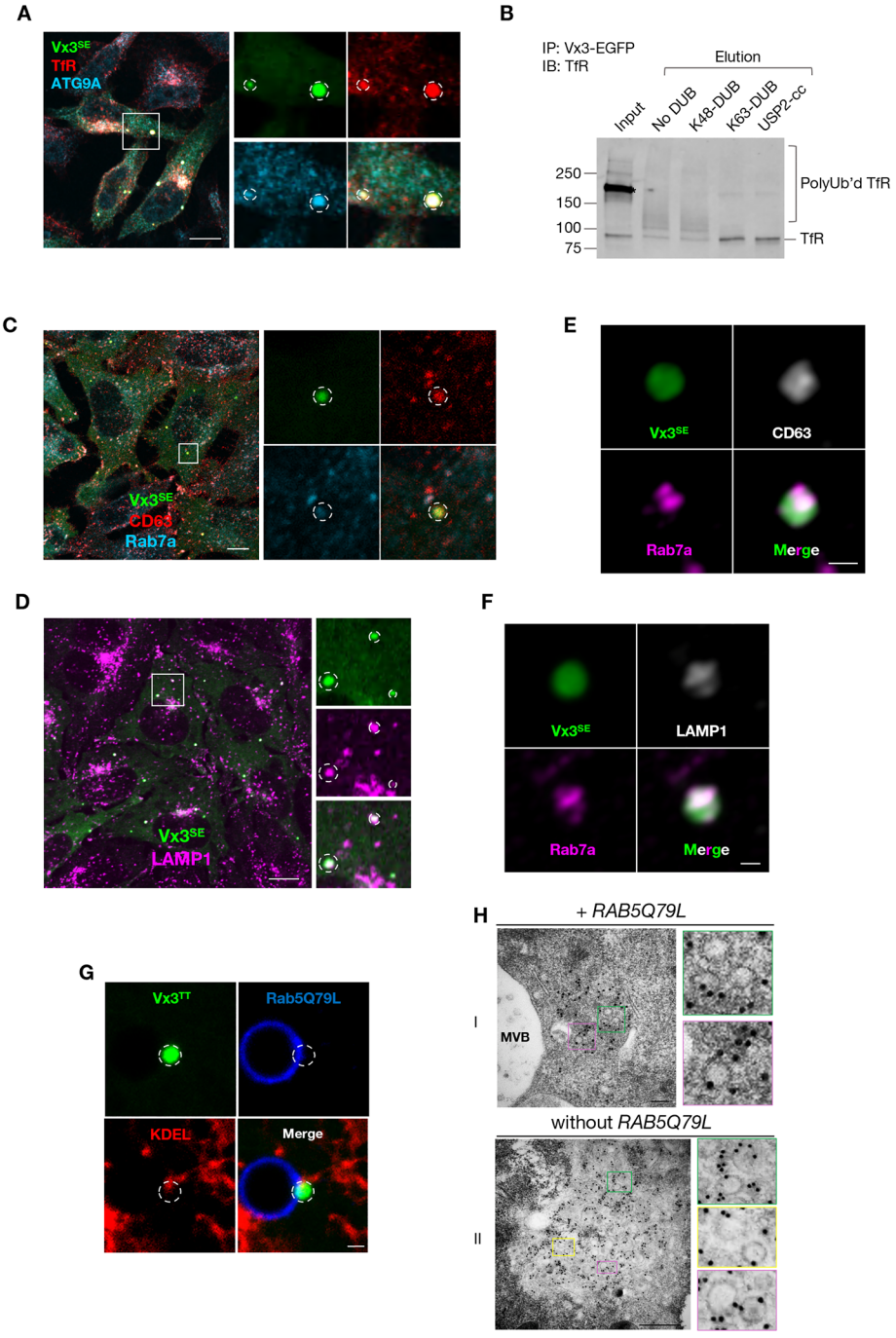

FIGURE 3: Vx3-EGFP expression causes accumulation of K63-polyubiquitylated cargo of plasma membrane origin in close proximity to endolysosomes. (A) Vx3-EGFP foci contain TfR. HeLa-Vx3^{SE} after 24 h Dox treatment (Vx3, *green*) were stained with anti-TfR (*red*) and anti-ATG9A (*light blue*) antibodies. A representative Vx3 focus is shown in the magnified panels. The dashed circle around a Vx3 focus in the magnified region is projected onto the other channels to indicate colocalization. Scale bar: 10 µm. (B) Endogenous TfR is K63-polyubiquitylated. HeLa-Vx3^{SE} cells induced with Dox for 48 h before subjecting whole cell lysates to Vx3 immunoprecipitation with GFP-Trap. Elutions were treated with linkage-specific or nonspecific DUBs and analyzed by immunoblotting with anti-TfR. Ubiquitylated TfR appears as a high molecular weight smear. Residual dimeric TfR, indicated by an asterisk, is due to incomplete disulfide reduction of the sample. (C) Vx3-EGFP foci colocalize with late endosomal markers. HeLa-Vx3^{SE} cells induced for 24 h were analyzed for Vx3 (*green*) and costained with anti-CD63 (*red*) and anti-Rab7a (*light blue*). The dashed circle around a Vx3 focus is projected onto the other channels to visualize colocalization. Scale bar: 10 µm. (D) Vx3-EGFP foci colocalize with the lysosomal marker LAMP1. Single *z*-section image of HeLa cells expressing Vx3^{SE} (*green*) treated with Dox for 24 h and stained with an anti-LAMP1 (*magenta*). The dashed circle around a Vx3 focus projected onto the LAMP1 channel to visualize colocalization. Scale bar: 10 µm. (E and F) Airyscan images (single *z*-section) of a Vx3–CD63–Rab7a (E) or Vx3–LAMP1–Rab7a (F) focus from a HeLa-Vx3^{SE} cell treated with Dox for 24 h and stained with an anti-CD63 (E) or anti-LAMP1 (F) and anti-Rab7a. Vx3 (*green*), CD63 or LAMP1 (*white*), Rab7a (*magenta*). Scale bars: 1 µm. (G) Vx3-GFP

S3). Knockdown of VPS35, a core subunit of the retromer complex, or WASH1, a core component of the WASH complex that facilitates actin-mediated cargo sorting and vesicle trafficking (Derivery *et al.*, 2009; Hao *et al.*, 2013; Zavodszky *et al.*, 2014), results in mislocalization of ATG9A to the perinuclear region of the cell (Figure EV5G), consistent with previous reports (Zavodszky *et al.*, 2014). We found that Vx3 foci formation was decreased upon knockdown of the retromer core subunit VPS35 (Figure 5C). Similarly, siRNA targeting WASH1 also reduced Vx3 foci formation (Figure 5C). These results indicate that perturbation of ATG9A trafficking alters formation of Vx3 foci. Trafficking of ATG9A to recycling endosomes occurs via clathrin-positive carriers using the adaptor protein complex AP2 (Popovic and Dikic, 2014; Imai *et al.*, 2016). We found that knockdown of AP2A results in ATG9A mislocalization and reduced Vx3 foci (Figure 5D). Previous work also indicated that in yeast trafficking of Atg9 from the Golgi during autophagosome formation requires the multimeric exocyst complex (Geng *et al.*, 2010). In mammals, the exocyst complex has been reported to function as a tether of secretory post-Golgi vesicles at the plasma membrane (Pereira *et al.*, 2023). We found that loss of EXOC8, a subunit of the exocyst complex, alters ATG9A trafficking and reduces Vx3 signal in VMP1-iRFP foci (Figure EV5H). In contrast, disruption of the TRAPPIII machinery, known to mediate the retrieval of ATG9A vesicles from recycling endosomes to the Golgi apparatus (Imai *et al.*, 2016; Lamb *et al.*, 2016), results in accumulation of Vx3 foci (Figures EV5I and EV5J). These results strongly suggest that trafficking of Vx3-trapped K63-polyubiquitylated transmembrane proteins requires ATG9A but not other core autophagy machinery.

During selective autophagy, several cargo receptors function in part via interactions with (poly)ubiquitin signals (Adriaenssens *et al.*, 2022); we had observed colocalization of Vx3 with two of these receptors, p62/SQSTM1 and NBR1 (Figures 2C, EV1B, and EV2A; Supplemental Dataset S1). Individual knockdown of either p62/SQSTM1 or NBR1 alone did not affect Vx3 foci abundance (Supplemental Dataset S3). To test whether other autophagy cargo receptors are needed or play redundant roles for Vx3 foci formation, we employed a previously described HeLa cell line (HeLa penta-KO) deficient in the five receptor proteins p62/SQSTM1, NBR1, OPTN, NDP52, and TAX1BP1 (Lazarou *et al.*, 2015). Transiently-expressed Vx3 in HeLa penta-KO cells showed similar foci localization when compared with control HeLa cells (Figure 5E), indicating that neither p62/SQSTM1 nor the other major autophagy receptor proteins have a major role in Vx3-EGFP foci formation. The Vx3-EGFP foci that appear in HeLa penta-KO cells also stain for ATG9A (Figure EV5K), suggesting that autophagy cargo receptors are not required for ATG9A recruitment to such compartments. Altogether, these results show that Vx3-EGFP foci formation requires neither LC3 nor any of the major autophagy cargo receptors.

Our discovery that Vx3 foci formation depends on ATG9A trafficking offered additional opportunities to explore ubiquitin E2 or E3 enzymes that may be required for their formation. For this purpose, we employed RNAi to knockdown a subset of ubiquitin E2 or E3 enzymes that have been linked to endomembrane trafficking and K63-polyubiquitylation (Supplemental Dataset S3). The E2 ubiquitin-conjugating enzymes UBE2O and UBE2N are known to assemble K63-polyUb (Ye and Rape, 2009; Hao *et al.* 2013). We found that knockdown of UBE2O or UBE2N reduced Vx3 foci (Supplemental Dataset S3). Based on previous reports indicating a key role for yeast Rsp5 in mediating K63-polyubiquitylation of plasma membrane proteins (Piper *et al.*, 2014), we investigated members of the human Nedd4 family of HECT E3 ligases, which have been reported to regulate various ubiquitin-mediated protein sorting processes at the plasma membrane and Golgi (Sicari *et al.*, 2022). We found that siRNA-based depletion of the E3 ligase NEDD4L (also known as NEDD4-2) caused a decrease in Vx3 foci formation (Figure EV5L), an effect not seen upon knockdown of other members of the Nedd4 family (Figure EV5L; Supplemental Dataset S3), suggesting that NEDD4L contributes to K63-polyubiquitylation of transmembrane protein cargos that are targeted to the Vx3/ATG9A pathway.

DISCUSSION

Transmembrane proteins that are internalized from the plasma membrane via the endocytic pathway can either be recycled to the cell surface or directed to lysosomes for degradation (Huotari and Helenius, 2011). Several lines of evidence have implicated K63-polyUb in regulating various aspects of lysosome-related membrane trafficking either through MVB or selective autophagy pathways (Erpapazoglou *et al.*, 2014; Dósa and Csizmadia, 2022). Given the functional versatility of the K63-polyUb modification, different readers or receptor proteins must contribute to the selection of a subset of K63-polyubiquitylated conjugates to direct their downstream fates. Transmembrane endocytic cargo is typically marked by K63-polyUb and recognized by low-affinity UBDs contained within ESCRT components (Raiborg and Stenmark, 2009; Shields and Piper, 2011; Piper *et al.*, 2014). Additionally, affinity and specificity could be increased by protein homo- or hetero-oligomerization that would boost the recognition of K63-polyUb. For example, cooperative binding of the ESCRT-0 proteins (e.g., Hrs and STAM) (Lange *et al.*, 2012) or the presence of multiple UIMs within Eps15 (Polo *et al.*, 2002; Sims and Cohen, 2009) have been postulated to enhance binding avidity and specificity towards K63-polyubiquitylated transmembrane proteins to elicit the downstream segregation of cargo into intraluminal vesicles. On the other hand, recognition of K63-polyubiquitylated cargo (e.g., aggregated proteins, invading bacteria, damaged organelles) in selective autophagy seems to be achieved by the ability of p62/SQSTM1 to form oligomers with NBR1 (Kirkin, Lamark *et al.*, 2009), thereby increasing the effective affinity for K63-polyUb to sequester cargo into autophagosomes.

In this study, we uncovered an unexpected role of ATG9A in the degradation of K63-polyUb–modified membrane proteins. Our data support a model (Figure 6) in which, by tightly binding to K63-polyUb, Vx3 prevents degradation of plasma membrane

foci are found near enlarged endolysosomes. Single frame from Supplemental Video S1 of HeLa cells transiently cotransfected with BFP-KDEL (*red*), Vx3^{TT} (*green*), and mCherry-Rab5Q79L (*blue*). The dashed circle around a Vx3 focus is projected onto the other channels to visualize juxtaposition with KDEL (i.e., ER tubule) or Rab5Q79L (i.e., endolysosome). Scale bar: 1 µm. (H) Immunoelectron microscopy shows that vesicles containing Vx3-EGFP are alongside enlarged endolysosomes. Distribution of immunogold-labeled Vx3 was evaluated in HeLa-Vx3^{SE} with (image I) or without (image II) mCherry-Rab5Q79L. Images show localization of immunogold-labeled Vx3 within a cluster of vesicles. Magnified areas show anti-GFP immunogold particles seen at the cytoplasmic side of the Vx3^{SE}-containing membranes. Scale bars: 0.1 µm (image I) or 0.5 µm (image II).

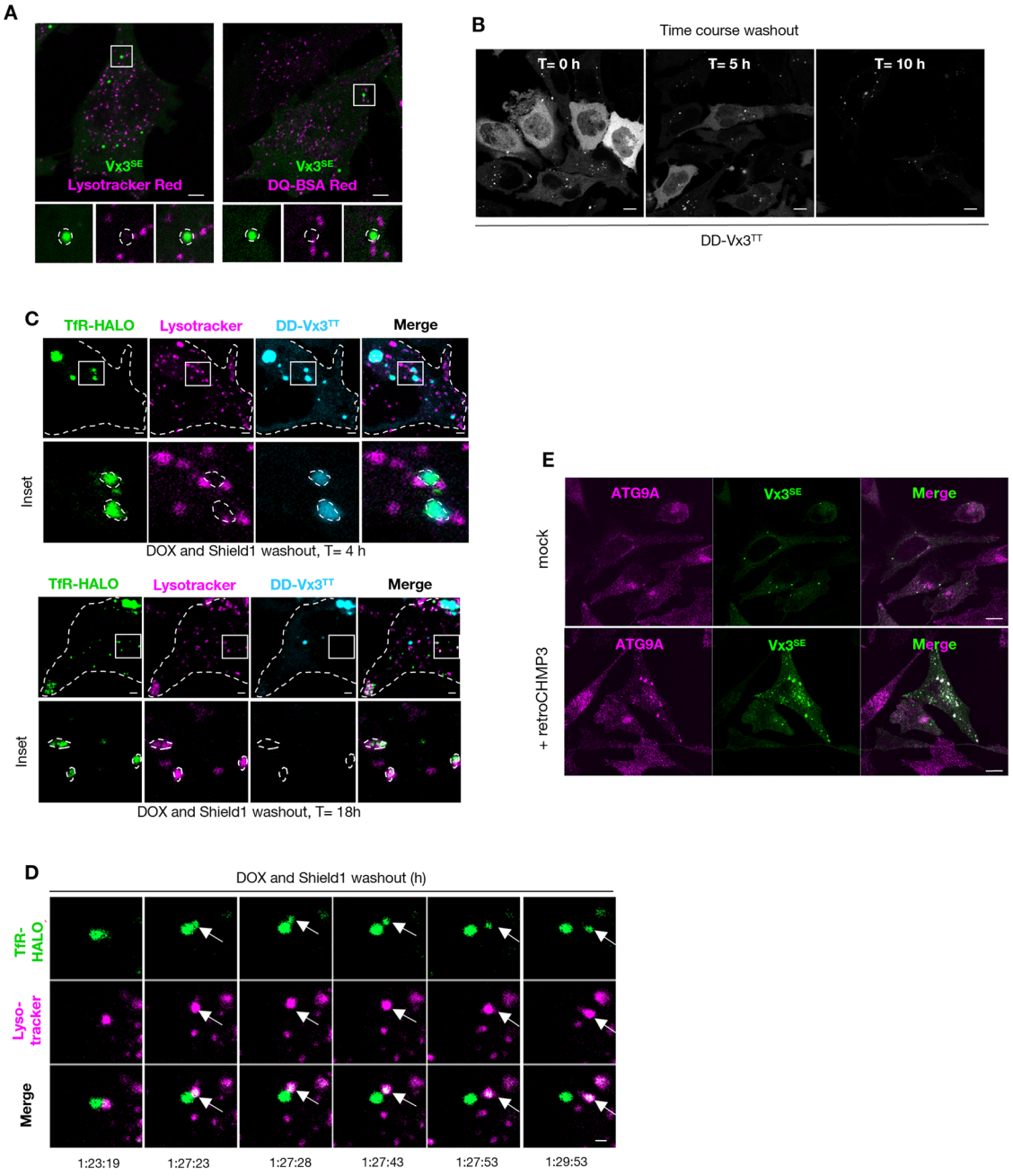

FIGURE 4: Vx3-EGFP expression inhibits delivery of K63-polyubiquitylated transmembrane protein cargo to endolysosomes (A) Vx3-EGFP foci do not colocalize with active lysosomes. HeLa-Vx3^{SE} cells (Vx3, *green*) were cultured with Dox for 24 h and then treated with 50 nM Lysotracker Red (*magenta*) for 1 h or pulsed with 10 μg/ml DQ-BSA Red (*magenta*) for 1 h and chased with fresh medium for 3 h before fixation. Insets show no colocalization of Vx3 foci (*green*) with either Lysotracker or DQ-BSA Red (*magenta*). Scale bars: 5 μm. (B) Time course (0, 5, and 10 h) of Vx3-EGFP (*white*) disappearance from HeLa FRT cells transfected with DD-Vx3^{TT}. HeLa FRT cells were treated with 1 ng/mL Dox for 12 h and then 10 μM Shield1 was added for another 12 h to promote DD-Vx3^{TT} expression and stabilization. At T = 0 h, Dox and Shield1 were washed out and DD-Vx3-EGFP fluorescence was monitored. Representative maximum projection images of the cells show nearly complete loss of Vx3 between 5 and 12 h. Scale bars: 2 μm. (C) TfR-containing vesicles released by Vx3-EGFP degradation traffic to the lysosomes. HeLa FRT were cotransfected with DD-Vx3^{TT} and TfR-HALO and treated with Dox and Shield1 as in B. After 24 h, cells were rinsed three times in PBS for drug washout and cultured in medium containing 100 nM PA-JF646 Halo ligand and 25 nM Lysotracker Red. At 4 h after washout, TfR-HALO colocalizing with selected DD-Vx3^{TT} foci (inset boxes) was photoactivated and monitored over time. Two representative maximum projection images and corresponding insets from one cell show that, after ~18 h drug washout, DD-Vx3^{TT} (*light blue*) was largely degraded and the previously colocalized TfR-HALO (*green*) overlapped extensively with Lysotracker (*magenta*). Dashed lines mark the cell contours, and outlines of the TfR-HALO foci are projected onto the other panels to visualize colocalization with DD-Vx3^{TT} and Lysotracker. Scale bars: 2 μm. (D) Time lapse images showing delivery of TfR to the lysotracker-positive vesicles. Live-cell imaging of HeLa FRT cells

proteins that are directed to lysosomes via an ATG9A-dependent vesicular pathway that is distinct from canonical autophagy routes. Key characteristics of this pathway are (i) the plasma membrane origin of the cargo and its modification with K63-polyUb, (ii) trafficking to lysosomal compartments is the final destination of the K63-polyubiquitylated cargo, and (iii) clustering of K63-polyubiquitylated cargo depends on ATG9A trafficking. We elaborate upon these points below.

K63-polyubiquitylation signals vesicular transport of cargo to lysosomes via an ATG9A-associated pathway

Several features of the Vx3-blocked vesicular transport pathway (Figure 6) are distinct from either the MVB pathway or selective autophagy. Unlike those classic pathways, we found that Vx3 leads to clustering of mixed populations of single- or double-membrane vesicles containing K63-polyUb–modified cargo or ATG9A. The K63-polyUb–modified cargo appear to reside on vesicles distinct from those containing ATG9A, with potentially different origins: that is, the plasma membrane for TfR and the endoplasmic reticulum for the VMP1-positive aggregates. Furthermore, results using both fluorescence and electron microscopy show that the clusters of vesicles decorated by K63-polyUb also contain markers of late endosomes such as Rab7a or LAMP1, and they are often found close to active lysosomes. By using an inducible system to release K63-polyUb signals bound by Vx3, we were able to identify processes immediately downstream of the Vx3-imposed block. Upon removal of Vx3, K63-polyubiquitylated cargo is rapidly delivered to acidic lysosomes, while the ATG9A vesicles dissociate.

Interestingly, we found that EGFR, a classic cargo of the MVB pathway (Duncan *et al.*, 2006; Lauwers *et al.*, 2009; Huang *et al.*, 2013; Tsuchiya *et al.*, 2018), colocalized with Vx3 foci upon stimulation of cells with the EGF ligand. This observation suggests that the binding of Vx3, which presumably blocks interaction of K63-polyUb reader(s), reroutes cargo to an alternative pathway that requires ATG9A and culminates in lysosomal delivery. Perturbation of the ESCRT machinery promoted further accumulation of K63-polyubiquitylated cargo trapped by Vx3 and colocalizing with ATG9A. These findings suggest that inhibition by Vx3 diverts at least some K63-polyubiquitylated cargo from ESCRT to an alternative lysosomal pathway (Figure 6). A previous electron microscopy study reported that disruption of ESCRTs leads to accumulation of nonmembrane-bound compartments positive for p62/SQSTM1 that were also comprised of single- and double-membrane vesicles (Filimonenko et al., 2007). Similar clusters of vesicles reminiscent of both endolysosomal and autophagosomal structures have been reported in other studies (Kishi-Itakura *et al.*, 2014; O'Loughlin *et al.*, 2020; Kuchitsu *et al.*, 2023). Recently, degradation of protein aggregates within nonmembrane-bound clusters of vesicles containing LAMP1 was observed in mouse oocytes; these were named endolysosomal vesicular assemblies (ELVAs) (Zaffagnini *et al.*, 2024). Thus, the Vx3-induced degradative pathway for membrane proteins of plasma membrane origin we describe here has ultrastructural features that are similar to ELVAs and the vesicular assemblies containing ubiquitin, p62/SQSTM1, and ATG9A reported previously.

A fraction of plasma membrane proteins is captured with Vx3

Using Vx3 to isolate K63-polyubiquitylated conjugates under stringent conditions, our mass spectrometry (MS) analyses identified proteins in which ~70% are localized to membranes or contain transmembrane domains (Supplemental Dataset S2); these are likely to be modified with K63-polyUb. Among the cell surface proteins we identified, many have been extensively characterized with respect to intracellular trafficking and many are found in recycling endosomes. This is the case for TfR, a prototypical cell surface receptor that cycles between the plasma membrane and endosomes (Ullrich *et al.*, 1996; Mayle *et al.*, 2012). We have shown that a small fraction of TfR is a *bona fide* K63-polyubiquitylated cargo that can be sequestered by Vx3 and is directed to lysosomes for degradation via ATG9A-associated vesicular transport. Importantly, only a minor population of intracellular TfR was found to be marked by Vx3, suggesting that features of either the cargo (i.e., the TfR proteins selected) or the membrane that contains the cargo must direct trafficking to this alternative pathway.

Whereas ubiquitin-dependent quality control pathways such as ERAD (Christianson *et al.*, 2023) and ER-phagy (Rudinskiy and Molinari, 2023) handle most misfolded transmembrane proteins at the ER, there are few documented quality control pathways for proteins that traffic through the endolysosomal system (Okiyoneda *et al.*, 2010, 2018; Falk *et al.*, 2014). Our results show that Vx3 foci containing TfR also colocalized with a VMP1-iRFP fusion protein but not endogenous VMP1. VMP1 is an ER-resident multispanning membrane protein implicated in early stages of autophagosome formation. We found that appending a fluorescent protein to the VMP1 C-terminus causes it to aggregate, in agreement with previous reports (Ropolo *et al.*, 2007; Itakura and Mizushima, 2010; Karanasios *et al.*, 2016; Zhao *et al.*, 2017; Renna *et al.*, 2023). Therefore, the localization of VMP1-iRFP into cytoplasmic inclusions that are bound by Vx3 suggests that protein aggregation might also elicit this ATG9-dependent pathway to eliminate faulty transmembrane proteins. It is possible that ATG9A vesicle recruitment onto VMP1 aggregates represents an early aborted attempt to engage the autophagy machinery for clearing these trapped vesicular aggregates, as indicated by the presence of p62/SQSTM1, NBR1, and LC3. Additional studies will be needed to identify the specific upstream signal(s) that promote the K63-polyubiquitylation. For the cargo of plasma membrane origin identified here, we have provided evidence that the Nedd4-2 E3 ligase is a likely candidate that generates the K63-polyUb signal.

Our proteomics analyses identified several proteins that are associated with plasma membrane microdomains containing cholesterol and sphingolipid enriched lipid rafts, including CAV-1, Integrin beta-1, MHC-I, TfR, and STOM (Supplemental Dataset S2). Caveolae-dependent sorting of membrane components at

cotransfected with DD-Vx3^{TT} and TfR-HALO and treated with Dox and Shield1 as in A. After drug washout, cells were incubated with 25 nM Lysotracker Red; foci that showed TfR-HALO colocalizing with Vx3 foci were photoactivated and then imaged at 1 frame every 5 s. Representative montages of single z-section time-lapse images show mobilization of photoactivated TfR-HALO (*green*) to Lysotracker-positive signals (*magenta*) starting ~80 min after drug washout); also see Supplemental Video S2. *White* arrows indicate the transfer of TfR from the original DD-Vx3^{TT}-stabilized cluster to a lysosome. Scale bar: 1 µm. (E) ESCRT inhibition results in accumulation of cytoplasmic Vx3-EGFP foci. HeLa-Vx3^{SE} cells (Vx3, *green*) were transfected with a vector containing retroCHMP3 or an empty vector (*mock*) for 24 h before treatment with Dox for an additional 24 h. Cells were stained with an anti-ATG9 (*magenta*). Scale bar: 10 µm.

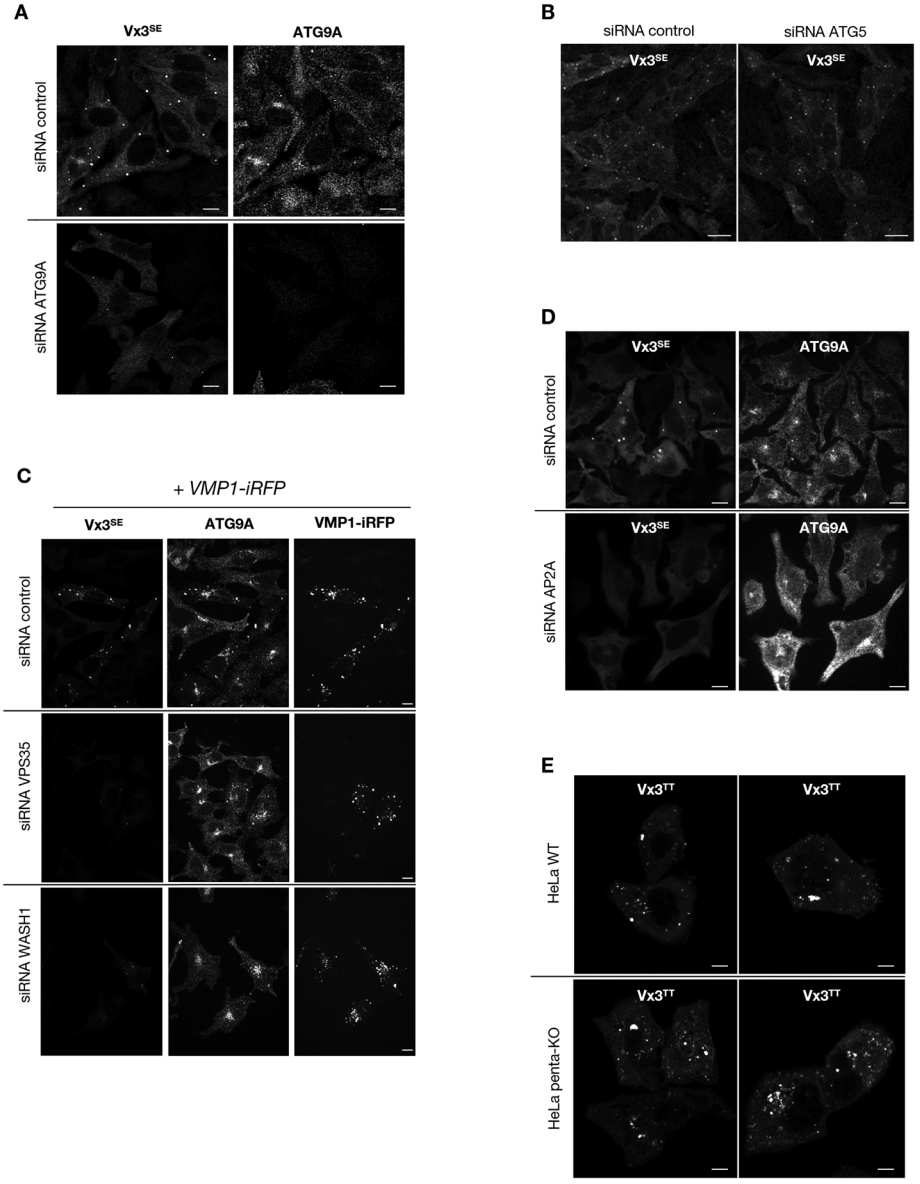

FIGURE 5: Among core components of the machinery needed for macroautophagy, only ATG9A is required for Vx3-EGFP foci formation (A) ATG9A depletion reduces Vx3-EGFP foci. HeLa-Vx3^{SE} cells were treated with either control siRNA or siRNA against ATG9A for 72 h. Vx3 expression was then induced by treatment with Dox for 24 h and cells were immunostained for ATG9A. Scale bar: 10 µm. (B) ATG5 knockdown does not affect Vx3 foci formation. HeLa-Vx3^{SE} cells were treated with either control siRNA or siRNA against ATG5 for 72 h. Vx3 expression was then induced by treatment with Dox for 24 h. Scale bar: 20 µm. (C) Perturbation of ATG9A trafficking reduces Vx3-EGFP foci formation. HeLa-Vx3^{SE}-VMP1 cells were treated with either control siRNA or siRNA against VPS35 or WASH1 for 72 h. Vx3 expression was induced for 24 h with Dox. Cells were stained with anti-ATG9A antibody (middle column). VMP1-iRFP localization into cytoplasmic inclusions is not affected by VPS35 or WASH1 knockdown. Scale bar: 10 µm. (D) Disruption of the clathrin adapter AP2A interferes with Vx3-EGFP foci formation. HeLa-Vx3^{SE} cells were treated with either control siRNA or siRNA against AP2A for 72 h. Vx3 expression was induced for 24 h with Dox. Cells were stained with anti-ATG9A antibody. Scale bar: 10 µm. (E) Vx3-EGFP foci formation does not require the five autophagy cargo receptors p62/SQSTM1, NBR1, OPTN, TAX1BP1, NDP52. penta-KO, and WT HeLa cells were transiently transfected with Vx3^{TT} for 24 h. The absence of p62/SQSTM1, NBR1, OPTN, TAX1BP1, and NDP52 does not affect Vx3 localization into cytoplasmic foci. Scale bar: 10 µm.

the plasma membrane, endosomes, or Golgi can cluster membrane proteins or lipids that would then pinch off for vesicular transport (Levental *et al.*, 2020; Sapoń *et al.*, 2023). Interestingly, a role for cholesterol in clustering of STING at the Golgi has been described (Kemmoku *et al.*, 2024). Below we highlight the similarities between the trafficking path of activated STING and the ATG9A-associated pathway identified by Vx3. Thus, the delivery of K63-polyubiquitylated membrane proteins into lysosomes via caveolae might represent an alternative route for transport into lysosomes; trafficking through this route is enhanced by the

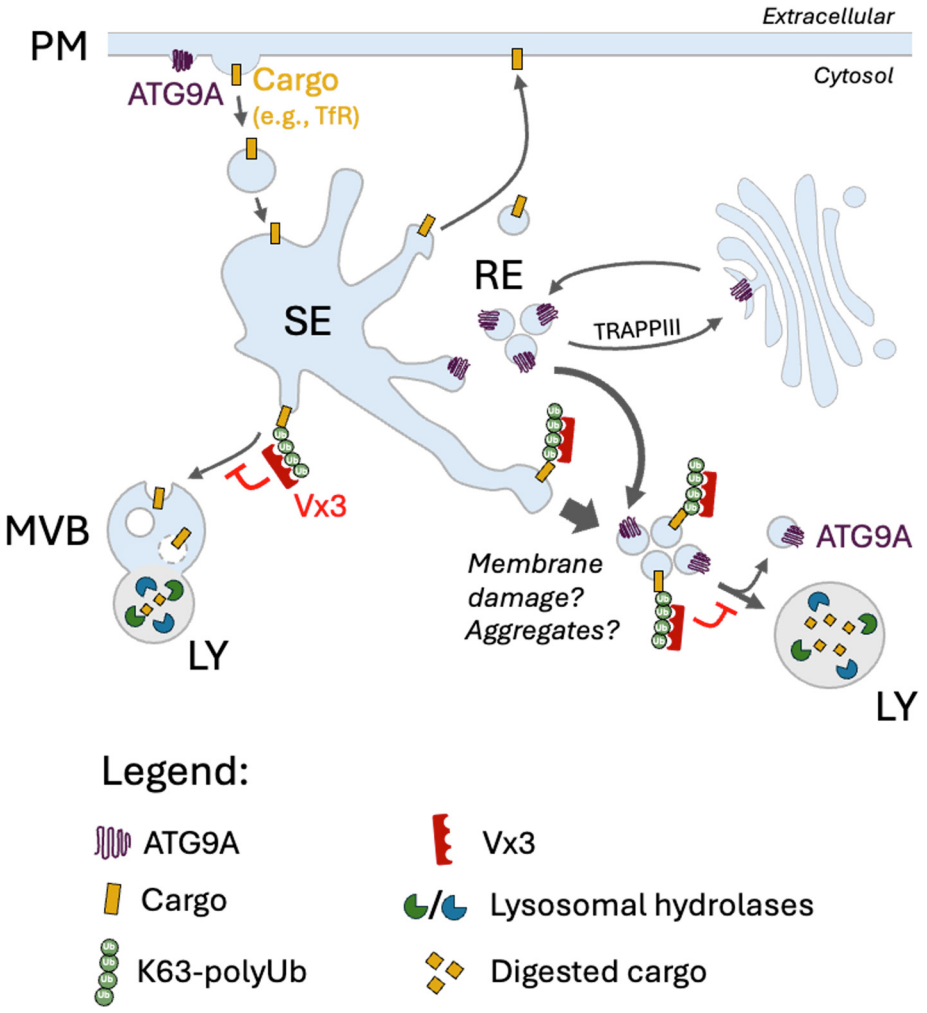

FIGURE 6: Model of K63-polyUb and ATG9A-assisted trafficking of plasma membrane proteins to lysosomes. Plasma membrane proteins (e.g., TfR, *yellow*) that are internalized into sorting endosomes (SE) via clathrin-mediated endocytosis are K63-polyubiquitylated (Ub chain, *light green*) to become degradative cargo for the ESCRT–MVB pathway. Vx3 causes accumulation of cargos destined for degradation into lysosomes (LY) via the MVBs (MVB-cargo segregated into intraluminal vesicles), most likely by direct competition with ESCRTs for binding to K63-polyUb (Ub chain, *light green*). This block reroutes the K63-polyubiquitylated cargos to an alternative lysosomal proteolysis pathway that depends on ATG9A (multipass membrane protein, *purple*) but not on other autophagy core machinery. We hypothesize that ATG9A-containing vesicles, which are distinct from the vesicles decorated by K63-polyUb, traffic to Vx3 foci from the recycling endosomes (RE) where they survey endocytosed cargo at the crossroad between protein recycling and degradation to triage aberrant lipids or proteins for lysosomal degradation.

Vx3-imposed block of ESCRT-dependent internalization of cargo into intraluminal vesicles of the MVBs.

Trafficking of K63-polyubiquitylated cargo is dependent on ATG9A

The most surprising finding from our study is that ATG9A is closely associated with K63-polyubiquitylated transmembrane proteins within the cytoplasmic clusters of vesicles induced by Vx3 expression. Superresolution microscopy indicated that ATG9A-positive vesicles do not localize precisely with K63-polyUb but rather are found adjacent to Vx3, suggesting that ATG9A is not directly modified by K63-polyUb. The absence of ATG9A among the polyubiquitylated proteins identified in our immunoprecipitation-MS analysis is consistent with this conclusion. We also showed that ATG9A is necessary for the formation of Vx3-EGFP foci—ATG9A depletion resulted in nearly complete absence of cytoplasmic inclusions containing K63-polyubiquitylated cargo. This effect was not a consequence of impaired autophagosome formation, as knockdown of LC3 or other autophagy proteins essential for phagophore nucleation or LC3 conjugation did not alter Vx3-EGFP foci formation.

ATG9A also plays roles outside macroautophagy (Claude-Taupin *et al.*, 2021; Vale-Costa *et al.*, 2023). In the innate immune response to double-stranded DNA, ATG9A is needed for trafficking of STING and assembly of a complex with TBK1 (Saitoh *et al.*, 2009). Notably, STING has been reported to be degraded via an alternative autophagic pathway (i.e., lysosomal microautophagy) involving invagination of single-membrane vesicles within lysosomes via a K63-polyUb and ESCRT-dependent mechanism (Kuchitsu *et al.*, 2023). We recently reported that Vx3 colocalizes with STING upon its activation (Fischer *et al.*, 2024). Thus, it is possible that STING is degraded via a similar pathway that we describe here for TfR. It was previously shown that STING activation induces LC3

lipidation onto single-membrane vesicles through a mechanism that is independent of canonical core autophagic components (Fischer *et al.*, 2020). Here we show that the Vx3-blocked vesicular transport pathway is dependent on ATG9A but not on other core autophagic machinery necessary for LC3 lipidation. Furthermore, our results indicate that additional signals such as membrane damage (e.g., induced by cationic lipids) or protein aggregation (e.g., induced by VMP1-iRFP overexpression) are needed to trigger LC3 lipidation on membranes residing within the Vx3/ATG9A vesicular clusters. Possibly, LC3 lipidation contributes to promoting fusion of vesicles decorated by K63-polyUb with lysosomes downstream to the Vx3's block. Interestingly, a similar autophagy-independent lysosomal transport requiring ESCRT and ATG9A but not LC3 lipidation was previously described for ferritin (Goodwin *et al.*, 2017). Degradation of ferritin also depends on TBK1, as inhibition of TBK1 affected ATG9A localization and lysosomal targeting of ferritin (Goodwin *et al.*, 2017). Further studies will be needed to determine if TBK1 is used to regulate ATG9A during Vx3 foci formation; notably, our siRNA-mediated knockdown screen for machinery contributing to Vx3-EGFP foci formation identified TBK1 as a likely factor (Supplemental Dataset S3).

Dependence of Vx3 foci formation on ATG9A was underscored by our finding that perturbing ATG9A trafficking can either increase or decrease Vx3 foci abundance. The retromer–WASH1 complex and the exocyst complex have been shown to regulate cycling of ATG9A vesicles through plasma membrane, recycling endosomes and the Golgi (Zavodszky *et al.*, 2014; Singh *et al.*, 2019). RNAi-mediated knockdown experiments showed that loss of either the retromer core subunit VPS35 or the WASH complex subunit WASH1 caused a nearly complete loss of Vx3 foci. Similarly, depletion of EXOC8, a component of the exocyst complex, reduced Vx3 foci formation. In contrast, knockdown of TRAPPC8, which leads to ATG9A accumulation in recycling endosomes (Imai *et al.*, 2016; Lamb *et al.*, 2016), increased Vx3 foci formation. Activated STING was previously shown to traffic through the recycling endosome and colocalize with ATG9A (Saitoh *et al.*, 2009; Kuchitsu *et al.*, 2023). These results suggest that the same population of ATG9A that associates with activated STING is involved in Vx3 foci accumulation.

We were surprised to find that formation of Vx3/ATG9A vesicular clusters does not depend on any of the five autophagy cargo receptors p62/SQSTM1, NBR1, OPTN, NDP52, and TAX1BP1. This is distinct from previous studies that have indicated that clustering of ubiquitylated cargo is mediated by p62/SQSTM1, OPTN, or NDP52 and occurs upstream of ATG9A recruitment (Zaffagnini *et al.*, 2018; Richard *et al.*, 2020; Yamano *et al.*, 2020; Turco *et al.*, 2021; Broadbent *et al.*, 2025). Because ATG9A interacts with lipids, ATG9A vesicles that traffic through various intracellular compartments may play a central role in the surveillance of membrane lipid or transmembrane protein damage by triaging them for either recycling to the plasma membrane or transport to lysosomes for degradation via a K63-polyUb dependent pathway. Thus, one possibility is that ATG9A facilitates cargo collection prior to delivery to lysosomes, potentially by promoting the clustering of cargo or its modification by K63-polyUb. Why ATG9A is needed for Vx3 foci formation, what is being delivered by ATG9A vesicles to the vesicular clusters marked by Vx3, and whether ATG9A directly interacts with K63-polyUb are key questions that remain to be answered in future studies. Although the alternative trafficking pathway that we observed is induced by the artificial expression of Vx3, it is possible that this pathway can become prominent in cells with compromised capacity to maintain proteostasis. For example, autophagy-related unconventional secretion of protein aggregates has been implicated in cell-to-cell transmission of the aggregates, contributing to neurodegenerative diseases (Noh *et al.*, 2022). Thus, the physiological significance of this K63-polyUb and ATG9A-dependent pathway remains to be discovered.

MATERIALS AND METHODS

Cell culture and generation of stable cell lines

HeLa, HEK293, Flp–In T-REx HeLa, and Flp–In T-REx 293 cells were maintained in DMEM (Life Technologies) supplemented with 10% (vol/vol) FBS (Atlas Biologicals), 2 mM L-glutamine (Hyclone), 100 U/mL penicillin (Hyclone), and 100 µg/ml streptomycin (Hyclone). Cell lines were regularly tested for *Mycoplasma* contamination using PCR Mycoplasma Detection Kit (G238, Applied Biological Materials Inc.). To generate stable cell lines, Vx3-EGFP was subcloned with N-terminal 3xFLAG tags into pcDNA5–FRT/TO and cotransfected with pOG44 recombinase-containing plasmid into parental Flp–In T-REx 293 or Flp–In T-REx HeLa cells, respectively (Invitrogen). Inducible stable cell lines were established following selection and clonal expansion in complete medium containing 0.3 mg/ml hygromycin. Clones were analyzed for inducible expression of Vx3-EGFP and its localization in cytoplasmic foci after addition of 1 µg/ml Dox for either 24 or 48 h.

VMP1 was amplified from the pMRXIP-hVMP1-GFP plasmid (a gift from N. Mizushima, University of Tokyo, Japan) and subcloned into pQCXIP (puromycin) retrovector as a fusion with C-terminal HA and iRFP (Addgene #45459; iRFP682 was a gift from V. Verkhusha, Albert Einstein College of Medicine) tags to generate HeLa stably expressing Dox-inducible 3xFLAG-Vx3-EGFP and transduced VMP1-HA-iRFP. Retroviruses for transduction were produced by transfection of Phoenix cells (a gift from J. DeLuca, Colorado State University) using Lipofectamine 2000 with 1 µg pVSV-G and 1 µg of pQCXIP-VMP1-HA-iRFP. Viruses were harvested 48 h after transfection, filtered (0.45 µm), and used with 4 µg/ml polybrene to infect Flp–In T-REx HeLa expressing 3xFLAG-Vx3-EGFP or 3xFLAG-Vx3NB-EGFP. Stably transduced HeLa cells were subsequently selected for growth with 1 µg/ml puromycin and subjected to clonal expansion.

The DD-tagged 3xFLAG-Vx3-EGFP was constructed by subcloning the FKBP12-variant destabilizing domain (i.e., FKBP12 E31G, F36V, R71G, K105E; ordered as a gene block from Integrated DNA Technologies, Inc.) upstream of the 3xFLAG sequence. To induce DD-Vx3-EGFP expression, the plasmid was transiently transfected into parental Flp–In T-REx HeLa for 24 h; Dox and 1 µM Shield-1 were added simultaneously for the indicated times to induce expression and localization of Vx3-EGFP into cytoplasmic foci.

ATG9A was cloned from cDNA into pmCherry-C2 or pFN21A HaloTag (HALO) vectors using In-Fusion cloning (Takarabio). TfR-HALO (in pFN21A backbone) was cloned from TfR-mCherry (Addgene #55144; a gift from M. Davidson, Florida State University). mCherry-Rab5 (Addgene #49201) and BFP-KDEL (Addgene #49150) were a gift from G. Voeltz, University of Colorado. Rab5 was mutated to introduce the Q79L mutation using the following pair of oligonucleotide primers by site-directed mutagenesis: 5′-GATACAGCTGGTCTAGAACGATACCATAGCCTAG-3′ (*Forward Primer*), 5′-GGTA TCGTTCTAGACCAGCTGTATCCCATATTTC-3′ (*Reverse Primer*). mCherry-Sec61b (Addgene #121160) was a gift from C. Mayr, Memorial Sloan Kettering Cancer Center.

Transfections, treatments, and autophagy induction

DNA plasmids were transfected using Lipofectamine 2000 or Lipofectamine 3000 according to manufacturer's instructions (Thermo Fisher Scientific). For RNAi treatment, HeLa-Vx3^{SE} cells grown in 24-well tissue culture plates (~5 × 10^4 cells/well) were transfected with 6 pmol siRNA with Lipofectamine RNAiMAX and phenotypes were assessed 72 h posttransfection. Where indicated, Vx3-EGFP expression was induced by the addition of 1 µg/ml Dox for 24 or 48 h. siGenome SMART pool siRNA against *ATG9A*, *VMP1*, *ATG5*, *VPS35*, *WASH1*, *USP8*, *ULK1*, *ATG14*, *Beclin1*, *ATG16L1*, *EXOC8*, *TRAPPC8*, *NEDD4*, *NEDD4L*, *p62/SQSTM1*, *NBR1*, *ABCD3*, *Myo6*, *Rab7a*, *RalB*, *SNAP25*, *STING*, *TBK1*, *TBC1D5*, *TOLLIP*, *UBE2N*, *UBE2O*, *UBE2V1*, *AMFR*, *GAN*, *HECW1*, *TRAF6*, *USP33*, *USP7*, *USP9x* were purchased from Dharmacon. Two premixed custom siRNAs against *AP2a1/2* were purchased from Sigma-Aldrich: 5′-GAGCAUGUGCACGCUGGCCAGCU-3′; 5′-AGCTGGCCAGCGTGCACATGCTC-3′.

To monitor autophagy of damaged membrane by fluorescence microscopy, HeLa-Vx3^{SE} were infected with RFP-containing *Salmonella* (a gift from J. Brumell, University of Toronto, Canada) for 1 h as described elsewhere (Zheng *et al.*, 2009), or treated by adding 3 µl Lipofectamine 2000 or Effectene for 4 h. For *Salmonella* growth assays performed in the presence or absence of Vx3-EGFP, HEK293-Vx3^{SE} cells were infected as previously described (Zheng *et al.*, 2009), lysed in 0.3% Triton X-100 in PBS and plated on LB agar plates at different times postinfection, and bacterial colonies were counted after incubation at +37°C overnight.

Immunostaining, fluorescent probes, and confocal microscopy

Cells grown on coverslips at <80% confluence were fixed with 2.5% paraformaldehyde in PBS for 10 min at +37°C, and preserved in PBS at +4°C. For immunostaining, unless otherwise specified, fixed cells were permeabilized with 0.1% Triton X-100 for 10 min at room temperature and blocked for 1 h with 1% BSA in PBS (blocking buffer) before incubation with primary antibodies diluted in blocking buffer for 2 h at room temperature or overnight at +4°C. The following antibodies were used for this study: anti-K63-polyUb (clone Apu3, Millipore; 1:400 dilution), anti-ATG9A (clone EPR2450[2], Abcam; 1:200 dilution), anti-p62/SQSTM1 (Abcam #56416; 1:500 dilution), anti-TfR/CD71 (clone CY1G4, BioLegend; 1:100 dilution), anti-LAMP1 (clone H4A3, Iowa Developmental Studies Hybridoma Bank; 1:100 dilution), anti-VMP1 (clone D6N4G, Cell Signaling Technology [CST]; 1:200), anti-ATG16L1 (clone D6D5, CST, 1:200 dilution), anti-Galectin-3 (clone A3A12, Abcam; 1:100 dilution), anti-NBR1 (clone 6B11, Abnova, 1:200 dilution), anti-MHC-I/HLA-A,B,C (clone W6/32, BioLegend; 1:100 dilution), CAV1-AF647 (clone 7C8, Santa Cruz Biotechnology; 1:50 dilution), anti-EEA1 (clone 14, BD Biosciences; 1:200 dilution), anti-GM130 (clone EP892Y, Abcam, 1:200 dilution), anti-TGN38 (clone 21-G, Santa Cruz Biotechnology; 1:200 dilution), anti-Sec31A (clone 32, BD Biosciences; 1:200 dilution), anti-calnexin (clone W17077C, BioLegend; 1:100 dilution). For anti-ATG9A antibody, incubation was 2 h at room temperature with the above described protocol. Staining with anti-LC3 (clone 4E12, MBL; 1:100 dilution) was done as reported previously (Sims *et al.*, 2012). For immunostaining with anti-ULK1 (clone H240, Santa Cruz Biotechnology, 1:200 dilution), anti-FIP200 (Proteintech #17250-1-AP,1:200 dilution), anti-WIPI2b (clone 2A2, Bio-Rad, 1:200 dilution), anti-Rab11 (clone D4F5, CST; 1:100 dilution), anti-CD63 (clone H5C6, BioLegend; 1:200 dilution), and anti-Rab7a (clone D95F2, CST; 1:200 dilution), we adapted a protocol described previously (Karanasios *et al.*, 2014). For immunostaining with anti-CAV-1 (AlexaFluor 647 conjugate; clone D46G3, CST; 1:200 dilution), cells were fixed in 100% cold methanol (precooled at −20°C) for 10 min at room temperature. An Olympus IX81 spinning disk confocal (CSU22 head) microscope with 100x/1.40 NA or 60x/1.42 NA objectives was used to acquire fixed-cell images with a Photometrics Cascade II CCD camera using SlideBook (Intelligent Imaging Innovations, Denver, CO, USA) software and processed with SlideBook software (Version 6.0.4). We also collected fixed-cell images and live-cell time-lapse images using a Zeiss LSM 880 confocal microscope equipped with both GAsP and Airyscan detectors using a plan-Apochromat 63x/NA 1.40 oil immersion objective. The Zen black software (Version 14.0.9.201) was used for image capture. The Processing and Analysis modules of the ZEN blue software (v.2.3.69.1000) were used to generate maximum intensity projection images of z-stacks. Airyscan superresolution images were acquired with the settings recommended by the manufacturer. After acquisition, Airyscan images were processed to enhance resolution using the Airyscan processing tool in ZEN Black software (Version 14.0.9.201). Images of Tetraspeck beads (Thermo Fisher Scientific) were employed as a reference for channel alignments of three-color images using ZEN Black.

For live-cell imaging studies, HALO-tagged constructs were labeled with 100 nM PA-JF646-Halo or 10 nM JF-549-Halo ligands, both gifts from Luke Lavis (Howard Hughes Medical Institute). Labeling occurred at +37°C, 5% CO_2 for 30 min, and cells were then washed three times with PBS before adding live-cell medium (FluorBrite DMEM supplemented with 10% FBS, 1% Penicillin-Streptomycin, and 2 mM L-Glutamine) for imaging. Endolysosomes were labeled for live-cell imaging using 10 µg/ml DQ-BSA Red (Invitrogen) or 50 nM Lysotracker Red (Invitrogen) for the indicated times.

Colocalization quantification and statistical analyses

For colocalization quantification in Figure 1D, images were processed in Slidebook 5.0 software (3i) as described previously (Bultema *et al.*, 2014). Quantification in Figures 1F and EV5C were performed with the Image Analysis Wizard module in Zen Blue software (v.2.3.69.1000) by applying a constant threshold of fluorescence intensity to mask LC3 puncta (Figure 1F), VMP1-iRFP puncta (for siRNA ATG9A condition in Figure EV5C) or Vx3-EGFP puncta (for siRNA VMP1 condition in Figure EV5C) in all the images analyzed. Quantification in Figure EV5A was performed by manually scoring the number of Vx3^{SE}-expressing cells containing at least 2 Vx3 foci over the total number of cells detected by DAPI staining. All the other colocalization analyses reported in Supplemental Dataset S1 were performed using Fiji (Image J) as described (Pike *et al.*, 2017). Mander's coefficients (M2) were calculated using the JaCoP colocalization plug-in. The numbers of total cells analyzed for each immunostaining experiment are reported in Supplemental Dataset S1.

Statistical calculations were performed with GraphPad Prism software and are described in the relevant figure legends. *P*-values are reported either in the graphs or indicated by an asterisk when they are considered significant (< 0.05).

Correlative light-electron microscopy (CLEM)

CLEM experiments were performed with HeLa-Vx3^{SE}-VMP1 cells transiently transfected with mCherry-ATG9A. The cells were grown on etched-grid glass bottom dishes (No. 1.5; MatTek Corporation). A two-step fixation protocol was used. The first round of

fixation was performed with 2% paraformaldehyde and 0.2% glutaraldehyde in 0.1 M sodium cacodylate buffer, pH 7.4. This low percentage of glutaraldehyde did not alter EGFP, mCherry, or iRFP fluorescence signals; therefore, cells triply-expressing Vx3-EGFP, mCherry-ATG9A, and VMP1-iRFP could be identified by fluorescence and differential interference contrast (DIC) microscopy using a 20X plan-Apochromat 20x/NA 0.8 objective to mark their positions relative to the etched grid. Next, 0.18-µm-thick z-section images of Vx3–ATG9A–VMP1-containing structures were obtained using the Zeiss Airyscan superresolution mode with a plan-Apochromat 63x/NA 1.40 oil immersion objective. Subsequently, cells were subjected to a second fixation procedure with Karnovsky fixative (2% paraformaldehyde/1.5% glutaraldehyde in 0.1 M sodium cacodylate buffer) for subsequent electron microscopy (EM) analysis.

The cells were stored in cacodylate buffer after fixation. For CLEM, the samples were processed as described (Gudmundsson *et al.*, 2019). Briefly, the cells were postfixed in 1% osmium tetroxide, dehydrated in ethanol, and flat-embedded in epoxy resin. Pyramids were trimmed using the etched grid as a guide to localize the cells of interest. Thin sections were cut with a diamond knife, picked up on Pioloform-coated one-slot grids, and stained with uranyl acetate and lead citrate. The sections were examined using a JEM-1400 electron microscope operating at 80 kV (JEOL, Tokyo, Japan).

Immunogold electron microscopy

HeLa-Vx3^{SE} cells were grown on 3 mm sapphire discs and transiently transfected with Rab5Q79L-mCherry for 24 h in the presence of 1 µg/ml Dox. First, sapphire discs were submerged in 2% sucrose plus 150 mM mannitol in complete medium. Cells were high-pressure frozen using a Wohlwend Compact 02 high pressure freezer (Technotrade International, Manchester, NH) as described previously (Meehl *et al.*, 2009). Frozen specimens were then freeze-substituted in anhydrous acetone containing 0.25% glutaraldehyde/0.1% uranyl acetate, embedded in Lowicryl HM20 resin, and UV-polymerized at low temperature (−45°C). Serial thin sections (60–80 nm) were cut using a Leica UCT ultramicrotome and collected on Formvar-coated nickel slot grids.

Thin sections were immunolabeled using an anti-GFP primary antibody in 1% nonfat milk powder blocking solution followed by a 15-nm gold-conjugated goat-anti-rabbit secondary antibody and poststaining with 2% (aqueous) uranyl acetate and Reynold's lead citrate (Meehl *et al.*, 2009). Sections were imaged on a FEI Tecnai T12 Spirit transmission electron microscope operated at 100 kV.

Immunoprecipitations, DUB assays, and Western blot analysis

HeLa-Vx3^{SE} cells were induced with 1 µg/ml Dox for 48 h and lysed in RIPA lysis buffer (50 mM Tris-Cl pH 7.6, 300 mM NaCl, 1% NP-40, 0.1% sodium deoxycholate, 1 mM EDTA) with 100 mM iodoacetamide, 4 mM 1,10-phenanthroline, and a protease inhibitor cocktail (P8340, Sigma-Aldrich). For co-IP, 15 µl GFP Trap agarose resin (ChromoTek) was added per 10-cm dish of cells. For binding, salt was increased to 500 mM NaCl and samples were incubated at +4°C for 1–2 h on a rotator. The resin was then washed with TBS (50 mM Tris pH 7.6, 150 mM NaCl). Samples were first eluted in 1.5x resin-volume of elution buffer (50 mM Tris pH 7.6, 3.3% SDS, 2 mM DTT) at room temperature (Elution 1) followed by a second round of elution with heating at +70°C (Elution 2). The majority of the ubiquitylated proteins were in Elution 1, and Elution 2 mostly contained Vx3-EGFP.

For deubiquitylation analyses, immunoprecipitated samples were digested while still bound to resin with purified recombinant DUB enzymes (i.e., OTUB1 [a gift from Cynthia Wolberger, Johns Hopkins University], GST-AMSH, or USP2-cc). After washing, the resin was resuspended in the digestion buffer (PBS pH 7.4, 0.3 mg/ml ovalbumin, 0.05% Brij35, 5 mM DTT) and incubated with 10 µM of specified DUB at +37°C for at least 1.5 h with shaking. The samples were then eluted with 2x Laemmli sample buffer.

For SDS–PAGE and Western blot analyses, heating of samples in gel loading buffer was avoided to prevent aggregation of membrane proteins. For immunoblotting, after transfer to PVDF membranes, primary antibodies against VMP1 (CST #12978), TfR (CST #131135), ATG9A (clone EPR2450[2], Abcam), Flag (F3165, Sigma), or Rab11 (clone D4F5, CST) were used at a 1:1000 dilution in 1% milk. The membranes were then labeled with fluorescent secondary antibodies and imaged with a LI-COR Biosciences Odyssey CLx scanner.

Mass spectrometry (MS) sample preparation

For MS analyses, four 10-cm dishes of cultured cells per condition were prepared. After co-IP, the elutions were precipitated in 80% acetone at −80°C overnight. The protein pellets were recovered by centrifuging at 10,000 × *g*, 4°C for 30 min and resuspended in 2x Laemmli sample buffer. To further fractionate the samples, 90% of the elutions were run on a 4–15% SDS–PAGE gradient gel (456-1083, Bio-Rad) to just beyond the stacking gel. The gel was then stained (0.05% Coomassie Blue R250, 10% acetic acid, 50% MeOH) for 1 h and destained (10% acetic acid, 50% MeOH) for 3 h with a solvent change each hour to remove SDS. Each gel lane was excised and cut into two pieces to separate proteins above and below ∼70 kDa. The gel pieces were dehydrated, reduced, and alkylated by sequential treatments with: 100% acetonitrile for 5 min at room temperature; 10 mM DTT with 0.1 M ammonium bicarbonate for 20 min at +55°C; 100% acetonitrile for 5 min, 55 mM iodoacetamide for 20 min at room temperature; and 100% acetonitrile for 5 min. The samples were then rehydrated and digested with 1:30 trypsin (V5111, Promega) in 0.1 M ammonium bicarbonate with 0.01% ProteaseMAX (V2071, Promega) at +37°C overnight. Afterward, the reactions were stopped with 10% trifluoroacetic acid (TFA) and the supernatants were collected. Remaining peptides left in the gel were further extracted by shaking the gel pieces in 50% acetonitrile and 0.1% TFA for 2 h and 100% acetonitrile for 5 min. These solutions were combined and dried down in a vacuum centrifuge and analyzed by LC-MS/MS at the University of California San Francisco Mass Spectrometry Facility essentially as described (Peters *et al.*, 2021). Briefly, tryptic peptides were analyzed on a QExactive Plus mass spectrometer (Thermo Fisher Scientific) connected to a NanoAcquity Ultra Performance UPLC system (Waters). A 15-cm EasySpray C18 column (Thermo Fisher Scientific) was used to resolve peptides (90-min 2–30% B gradient with 0.1% formic acid in water as mobile phase A and 0.1% formic acid in acetonitrile as mobile phase B, at a flow rate of 300 nl/min). MS was operated in data-dependent mode to automatically switch between MS and MS/MS.

ACKNOWLEDGMENTS

The authors are grateful for access to the Microscope Imaging Network Core Facility and James Bamburg, Laurie Minamide, O'Neil Wiggan, Tatsuya Morisaki and Barbara Bernstein at Colorado State University for assistance with confocal microscopy and many helpful discussions; Andrea Ambrosio and Santiago Di Pietro (Colorado State University) shared reagents and helped with colocalization

analyses. Garry Morgan at the University of Colorado Boulder Electron Microscopy Services Core Facility helped perform immunogold EM analyses; the CLEM experiments were done in the Electron Microscopy Unit of the Institute of Biotechnology, University of Helsinki. R.E.C. and T.Y. thank Alma Burlingame for hosting us at the UCSF Mass Spectrometry Facility where proteomics analyses were done under the guidance of Juan Oses-Prieto and Giselle M. Knudsen; we are grateful for their expert assistance and use of the facility instruments. We are grateful to Richard Youle for providing HeLa penta-KO and HeLa hATG8s-KO cell lines and Wes Sundquist for retroCHMP3 plasmid, as well as insightful discussions. We also thank Samantha Gumbin and Roni Levin-Konigsberg (Stanford University) for critical reading of the manuscript. This research was supported by American Heart Association Predoctoral Fellowship to F.S., Academy of Finland grant 286787 to E.-L.E, NIH grants (R01GM115997 and R21GM135818) to R.E.C and a Webb-Waring Biochemical Research Award to T.Y.

REFERENCES

Adriaenssens E, Ferrari L, Martens S (2022). Orchestration of selective autophagy by cargo receptors. Curr Biol 32, R1357–371.

Babu JR, Geetha T, Wooten MW (2005). Sequestosome 1/p62 shuttles polyubiquitinated tau for proteasomal degradation. J Neurochem 94, 192–203.

Banaszynski LA, Chen L-C, Maynard-Smith LA, Lisa Ooi AG, Wandless TJ (2006). A rapid, reversible, and tunable method to regulate protein function in living cells using synthetic small molecules. Cell 126, 995–1004.

Bjørkøy G, Lamark T, Brech A, Outzen H, Perander M, Overvatn A, Stenmark H, Johansen T (2005). p62/SQSTM1 forms protein aggregates degraded by autophagy and has a protective effect on huntingtin-induced cell death. J Cell Biol 171, 603–614.

Broadbent DG, Barnaba C, Perez GI, Schmidt JC (2023). Quantitative analysis of autophagy reveals the role of ATG9 and ATG2 in autophagosome formation. J Cell Biol 222, e202210078.

Broadbent DG, McEwan CM, Jayatunge D, Kaminsky EG, Tsang T-M, Poole DM, Naylor BC, Price JC, Schmidt JC, Andersen JL (2025). Ubiquitin-mediated recruitment of the ATG9A-ATG2 lipid transfer complex drives clearance of phosphorylated p62 aggregates. Mol Biol Cell 36, ar20.

Bultema JJ, Boyle JA, Malenke PB, Martin FE, Dell'Angelica EC, Cheney RE, Di Pietro SM (2014). Myosin vc interacts with Rab32 and Rab38 proteins and works in the biogenesis and secretion of melanosomes. J Biol Chem 289, 33513–33528.

Christianson JC, Jarosch E, Sommer T (2023). Mechanisms of substrate processing during ER-associated protein degradation. Nat Rev Mol Cell Biol 24, 777–796.

Claude-Taupin A, Jia J, Bhujabal Z, Garfa-Traoré M, Kumar S, Peixoto Duarte da Silva G, Javed R, Gu Y, Allers L, Peters R, *et al*. (2021). ATG9A protects the plasma membrane from programmed and incidental permeabilization. Nat Cell Biol 23, 846–858.

Derivery E, Sousa C, Gautier JJ, Lombard B, Loew D, Gautreau A (2009). The Arp2/3 activator WASH controls the fission of endosomes through a large multiprotein complex. Dev Cell 17, 712–723.

Dósa A, Csizmadia T (2022). The Role of K63-linked polyubiquitin in several types of autophagy. Biologia Futura 73, 137–148.

Duncan LM, Piper S, Dodd RB, Saville MK, Sanderson CM, Luzio JP, Lehner PJ (2006). Lysine-63-linked ubiquitination is required for endolysosomal degradation of class I molecules. EMBO J 25, 1635–1645.

Eapen VV, Swarup S, Hoyer MJ, Paulo JA, Harper JW (2021). Quantitative proteomics reveals the selectivity of ubiquitin-binding autophagy receptors in the turnover of damaged lysosomes by lysophagy. Elife 10, e72328.

Edelmann MJ, Iphöfer A, Akutsu M, Altun M, Gleria K, Kramer HB, Fiebiger E, Dhe-Paganon S, Kessler BM (2009). Structural basis and specificity of human otubain 1-mediated deubiquitination. Biochem J 418, 379–390.

Erpapazoglou Z, Walker O, Haguenauer-Tsapis R (2014). Versatile roles of k63-linked ubiquitin chains in trafficking. Cells 3, 1027–1088.

Falk MM, Kells RM, Berthoud VM (2014). Degradation of connexins and gap junctions. FEBS Lett 588, 1221–1229.

Filimonenko M, Stuffers S, Raiborg C, Yamamoto A, Malerød L, Fisher EMC, Isaacs A, Brech A, Stenmark H, Simonsen A (2007). Functional multivesicular bodies are required for autophagic clearance of protein aggregates associated with neurodegenerative disease. J Cell Biol 179, 485–500.

Fischer TD, Bunker EN, Zhu P-P, Guerroué FL, Hadjian M, Dominguez-Martin E, Scavone F, Cohen RE, Yao T, Wang Y, *et al*. (2024). STING induces HOIP-mediated synthesis of M1 ubiquitin chains to stimulate NF-κB signaling. EMBO J 44, 141–165.

Fischer TD, Wang C, Padman BS, Lazarou M, Youle RJ (2020). STING induces LC3B lipidation onto single-membrane vesicles via the V-ATPase and ATG16L1-WD40 domain. J Cell Biol 219, e202009128.

Friedman JR, Lackner LL, West M, DiBenedetto JR, Nunnari J, Voeltz GK (2011). ER tubules mark sites of mitochondrial division. Science 334, 358–362.

Fujita N, Morita E, Itoh T, Tanaka A, Nakaoka M, Osada Y, Umemoto T, Saitoh T, Nakatogawa H, Kobayashi S, *et al*. (2013). Recruitment of the autophagic machinery to endosomes during infection is mediated by ubiquitin. J Cell Biol 203, 115–128.

Geng J, Nair U, Yasumura-Yorimitsu K, Klionsky DJ (2010). Post-Golgi sec proteins are required for autophagy in Saccharomyces Cerevisiae. Mol Biol Cell 21, 2257–2269.

Gentili M, Liu B, Papanastasiou M, Dele-Oni D, Schwartz MA, Carlson RJ, Al'Khafaji AM, Krug K, Brown A, Doench JG, *et al*. (2023). ESCRT-dependent STING degradation inhibits steady-state and cGAMP-induced signalling. Nat Commun 14, 611.

Goodwin JM, Dowdle WE, DeJesus R, Wang Z, Bergman P, Kobylarz M, Lindeman A, Xavier RJ, McAllister G, Nyfeler B, *et al*. (2017). Autophagy-independent lysosomal targeting regulated by ULK1/2-FIP200 and ATG9. Cell Rep 20, 2341–2356.

Grimm JB, English BP, Choi H, Muthusamy AK, Mehl BP, Dong P, Brown TA, Lippincott-Schwartz J, Liu Z, Lionnet T, Lavis LD (2016). Bright photoactivatable fluorophores for single-molecule imaging. Nat Methods 13, 985–988.

Gudmundsson S, Kahlhofer J, Baylac N, Kallio K, Eskelinen E-L (2019). Correlative light and electron microscopy of autophagosomes. Methods Mol Biol 1880, 199–209.

Hao Y-H, Doyle JM, Ramanathan S, Gomez TS, Jia D, Xu M, Chen ZJ, Billadeau DD, Rosen MK, Potts PR (2013). Regulation of WASH-dependent actin polymerization and protein trafficking by ubiquitination. Cell 152, 1051–1064.

He C, Klionsky DJ (2009). Regulation mechanisms and signaling pathways of autophagy. Ann Rev Genet 43, 67–93.

Holzer E, Martens S, Tulli S (2024). The role of ATG9 vesicles in autophagosome biogenesis. J Mol Biol 436, 168489.

Huang F, Zeng X, Kim W, Balasubramani M, Fortian A, Gygi SP, Yates NA, Sorkin A (2013). Lysine 63-linked polyubiquitination is required for EGF receptor degradation. Proc Natl Acad Sci U S A 110, 15722–15727.

Hung Y-H, Chen LM-W, Yang J-Y, Yang WY (2013). Spatiotemporally controlled induction of autophagy-mediated lysosome turnover. Nat Commun 4, 2111.

Huotari J, Helenius A (2011). Endosome maturation. EMBO J 30, 3481–3500.

Husnjak K, Dikic I (2012). Ubiquitin-binding proteins: Decoders of ubiquitin-mediated cellular functions. Annu Rev Biochem 81, 291–322.

Imai K, Hao F, Fujita N, Tsuji Y, Oe Y, Araki Y, Hamasaki M, Noda T, Yoshimori T (2016). Atg9A trafficking through the recycling endosomes is required for autophagosome formation. J Cell Sci 129, 3781–3791.

Itakura E, Mizushima N (2010). Characterization of autophagosome formation site by a hierarchical analysis of mammalian Atg proteins. Autophagy 6, 764–776.

Jia J, Claude-Taupin A, Gu Y, Choi SW, Peters R, Bissa B, Mudd MH, Allers L, Pallikkuth S, Lidke KA, Deretić V (2020). Galectin-3 coordinates a cellular system for lysosomal repair and removal. Dev Cell 52, 69–87.e8.

Johansen T, Lamark T (2011). Selective autophagy mediated by autophagic adapter proteins. Autophagy 7, 279–296.

Karanasios E, Stapleton E, Manifava M, Ktistakis NT (2014). Imaging autophagy. Curr Protoc Cytom 69, 12.34.1–12.34.16.

Karanasios E, Walker SA, Okkenhaug H, Manifava M, Hummel E, Zimmermann H, Ahmed Q, Domart M-C, Collinson L, Ktistakis NT (2016). Autophagy initiation by ULK complex assembly on ER tubulovesicular regions marked by ATG9 vesicles. Nat Commun 7, 12420.

Kemmoku H, Takahashi K, Mukai K, Mori T, Hirosawa KM, Kiku F, Uchida Y, Kuchitsu Y, Nishioka Y, Sawa M, Suzuki K (2024). Single-molecule localization microscopy reveals STING clustering at the trans-Golgi

network through palmitoylation-dependent accumulation of cholesterol. Nat Commun 15, 220.
Kirkin V, Lamark T, Sou Y-S, Bjørkøy G, Nunn JL, Bruun J-A, Shvets E, McEwan DG, Clausen TH, Wild PS, *et al*. (2009). A role for NBR1 in autophagosomal degradation of ubiquitinated substrates. Mol Cell 33, 505–516.
Kirkin V, McEwan DG, Novak I, Dikic I (2009). A role for ubiquitin in selective autophagy. Mol Cell 34, 259–269.
Kishi-Itakura C, Koyama-Honda I, Itakura E, Mizushima N (2014). Ultrastructural analysis of autophagosome organization using mammalian autophagy-deficient cells. J Cell Sci 127, 4089–4102.
Koerver L, Papadopoulos C, Liu B, Kravic B, Rota G, Brecht L, Veenendaal T, Polajnar M, Bluemke A, Ehrmann M, *et al*. (2019). The ubiquitin-conjugating enzyme UBE2QL1 coordinates lysophagy in response to endolysosomal damage. EMBO Rep 20, e48014.
Komander D, Rape M (2012). The ubiquitin code. Annu Rev Biochem 81, 203–229.
Kuchitsu Y, Taguchi T (2024). Lysosomal microautophagy: an emerging dimension in mammalian autophagy. Trends Cell Biol 34, 606–616.
Kuchitsu Y, Mukai K, Uematsu R, Takaada Y, Shinojima A, Shindo R, Shoji T, Hamano S, Ogawa E, Sato R, *et al*. (2023). STING signalling is terminated through ESCRT-dependent microautophagy of vesicles originating from recycling endosomes. Nat Cell Biol 25, 453–466.
Lamb CA, Nühlen S, Judith D, Frith D, Snijders AP, Behrends C, Tooze SA (2016). TBC1D14 regulates autophagy via the TRAPP complex and ATG9 traffic. EMBO J 35, 281–301.
Lange A, Castañeda C, Hoeller D, Lancelin J-M, Fushman D, Walker O (2012). Evidence for cooperative and domain-specific binding of the signal transducing adaptor molecule 2 (STAM2) to Lys63-linked diubiquitin. J Biol Chem 287, 18687–18699.
Lauwers E, Jacob C, André B (2009). K63-linked ubiquitin chains as a specific signal for protein sorting into the multivesicular body pathway. J Cell Biol 185, 493–502.
Lazarou M, Sliter DA, Kane LA, Sarraf SA, Wang C, Burman JL, Sideris DP, Fogel AI, Youle RJ (2015). The ubiquitin kinase PINK1 recruits autophagy receptors to induce mitophagy. Nature 524, 309–314.
Lee J-A, Beigneux A, Ahmad ST, Young SG, Gao F-B (2007). ESCRT-III dysfunction causes autophagosome accumulation and neurodegeneration. Curr Biol 17, 1561–1567.
Lefebvre C, Renaud L, Emmanuel C (2018). ESCRT and autophagies: endosomal functions and beyond. Semin Cell Dev Biol 74, 21–28.
Levental I, Levental KR, Heberle FA (2020). Lipid rafts: Controversies resolved, mysteries remain. Trends Cell Biol 30, 341–353.
Maeda S, Yamamoto H, Kinch LN, Garza CM, Takahashi S, Otomo C, Grishin NV, Forli S, Mizushima N, Otomo T (2020). Structure, lipid scrambling activity and role in autophagosome formation of ATG9A. Nat Struct Mol Biol 27, 1194–1201.
Matoba K, Kotani T, Tsutsumi A, Tsuji T, Mori T, Noshiro D, Sugita Y, Nomura N, Iwata S, Ohsumi Y, *et al*. (2020). Atg9 is a lipid scramblase that mediates autophagosomal membrane expansion. Nat Struct Mol Biol 27, 1185–1193.
Mayle KM, Le AM, Kamei DT (2012). The intracellular trafficking pathway of transferrin. Biochim Biophys Acta 1820, 264–281.
McCullough J, Clague MJ, Urbé S (2004). AMSH is an endosome-associated ubiquitin isopeptidase. J Cell Biol 166, 487–492.
Meehl JB, Giddings TH, Jr, Winey M (2009). High pressure freezing, electron microscopy, and immuno-electron microscopy of tetrahymena thermophila basal bodies. Methods Mol Biol 586, 227–241.
Nathan JA, Kim HT, Ting L, Gygi SP, Goldberg AL (2013). Why do cellular proteins linked to K63-polyubiquitin chains not associate with proteasomes? EMBO J 32, 552–565.
Nguyen TN, Padman BS, Usher J, Oorschot V, Ramm G, Lazarou M (2016). Atg8 family LC3/GABARAP proteins are crucial for autophagosome–lysosome fusion but not autophagosome formation during PINK1/Parkin mitophagy and starvation. J Cell Biol 215, 857–874.
Niendorf S, Oksche A, Kisser A, Löhler J, Prinz M, Schorle H, Feller S, Lewitzky M, Horak I, Knobeloch K-P (2007). Essential role of ubiquitin-specific protease 8 for receptor tyrosine kinase stability and endocytic trafficking in vivo. Mol Cell Biol 27, 5029–5039.
Noh S, Hye Y, Kim J, Lee MG (2022). Autophagy-related pathways in vesicular unconventional protein secretion. Front Cell Dev Biol 10, 892450.
Okiyoneda T, Barrière H, Bagdány M, Rabeh WM, Du K, Höhfeld J, Young JC, Lukacs GL (2010). Peripheral protein quality control removes unfolded CFTR from the plasma membrane. Science 329, 805–810.
Okiyoneda T, Veit G, Sakai R, Aki M, Fujihara T, Higashi M, Susuki-Miyata S, Miyata M, Fukuda N, Yoshida A, *et al*. (2018). Chaperone-independent peripheral quality control of CFTR by RFFL E3 ligase. Dev Cell 44, 694–708.e7.
Olivas TJ, Wu Y, Yu S, Luan L, Choi P, Guinn ED, Nag S, De Camilli PV, Gupta K, Melia TJ (2023). ATG9 vesicles comprise the seed membrane of mammalian autophagosomes. J Cell Biol 222, e202208088.
O'Loughlin T, Kruppa AJ, Ribeiro ALR, Edgar JR, Ghannam A, Smith AM, Buss F (2020). OPTN recruitment to a Golgi-proximal compartment regulates immune signalling and cytokine secretion. J Cell Sci 133, jcs239822.
Orsi A, Razi M, Dooley HC, Robinson D, Weston AE, Collinson LM, Tooze SA (2012). Dynamic and transient interactions of Atg9 with autophagosomes, but not membrane integration, are required for autophagy. Mol Biol Cell 23, 1860–1873.
Pankiv S, Høyvarde Clausen T, Lamark T, Brech A, Bruun J-A, Outzen H, Øvervatn A, Bjørkøy G, Johansen T (2007). p62/SQSTM1 binds directly to Atg8/LC3 to facilitate degradation of ubiquitinated protein aggregates by autophagy. J Biol Chem 282, 24131–245.
Papadopoulos C, Kirchner P, Bug M, Grum D, Koerver L, Schulze N, Poehler R, Dressler A, Fengler S, Arhzaouy K, *et al*. (2017). VCP/p97 cooperates with YOD1, UBXD1 and PLAA to drive clearance of ruptured lysosomes by autophagy. EMBO J 36, 135–150.
Peng J, Schwartz D, Elias JE, Thoreen CC, Cheng D, Marsischky G, Roelofs J, Finley D, Gygi SP (2003). A proteomics approach to understanding protein ubiquitination. Nat Biotechnol 21, 921–926.
Pereira C, Stalder D, Anderson GSF, Shun-Shion AS, Houghton J, Antrobus R, Chapman MA, Fazakerley DJ, Gershlick DC (2023). The exocyst complex is an essential component of the mammalian constitutive secretory pathway. J Cell Biol 222, e202205137.
Peters JJ, Leitz J, Oses-Prieto JA, Burlingame AL, Brunger AT (2021). Molecular characterization of AMPA-receptor-containing vesicles. Front Mol Neurosci 14, 754631.
Pickart, CM (2001). Mechanisms underlying ubiquitination. Annu Rev Biochem 70, 503–533.
Pickart CM, Fushman D (2004). Polyubiquitin chains: Polymeric protein signals. Curr Opin Chem Biol 8, 610–16.
Pike JA, Styles IB, Rappoport JZ, Heath JK (2017). Quantifying receptor trafficking and colocalization with confocal microscopy. Methods 115, 42–54.
Piper RC, Dikic I, Lukacs GL (2014). Ubiquitin-dependent sorting in endocytosis. Cold Spring Harb Perspect Biol 6, a016808.
Polo S, Sigismund S, Faretta M, Guidi M, Capua MR, Bossi G, Chen H, De Camilli P, Fiore PPD (2002). A single motif responsible for ubiquitin recognition and monoubiquitination in endocytic proteins. Nature 416, 451–455.
Popovic D, Dikic I (2014). TBC1D5 and the AP2 complex regulate ATG9 trafficking and initiation of autophagy. EMBO Rep 15, 392–401.
Puri C, Gratian MJ, Rubinsztein DC (2023). Mammalian autophagosomes form from finger-like phagophores. Dev Cell 58, 2746–60.e5.
Puri C, Renna M, Bento CF, Moreau K, Rubinsztein DC (2013). Diverse autophagosome membrane sources coalesce in recycling endosomes. Cell 154, 1285–1299.
Radulovic M, Schink KO, Wenzel EM, Nähse V, Bongiovanni A, Lafont F, Stenmark H (2018). ESCRT-mediated lysosome repair precedes lysophagy and promotes cell survival. EMBO J 37, e99753.
Raiborg C, Bache KG, Gillooly DJ, Madshus IH, Stang E, Stenmark H (2002). Hrs sorts ubiquitinated proteins into clathrin-coated microdomains of early endosomes. Nat Cell Biol 4, 394–398.
Raiborg C, Stenmark H (2009). The ESCRT machinery in endosomal sorting of ubiquitylated membrane proteins. Nature 458, 445–452.
Renna FJ, Steinberg JHE, Gonzalez CD, Manifava M, Tadic MS, Orquera T, Vecino CV, Ropolo A, Guardavaccaro D, Rossi M, Vaccaro MI (2023). Ubiquitination is a novel post-translational modification of VMP1 in autophagy of human tumor cells. Int J Mol Sci 24, 12981.
Rheinemann L, Miller Downhour D, Bredbenner K, Mercenne G, Davenport KA, Schmitt PT, Necessary CR, McCullough J, Schmitt AP, Simon SM, *et al*. (2021). RetroCHMP3 blocks budding of enveloped viruses without blocking cytokinesis. Cell 184, 5419–31.e16.
Richard TJC, Herzog LK, Vornberger J, Rahmanto AS, Sangfelt O, Salomons FA, Dantuma NP (2020). K63-linked ubiquitylation induces global sequestration of mitochondria. Sci Rep 10, 22334.
Ropolo A, Grasso D, Pardo R, Sacchetti ML, Archange C, Lo Re A, Seux M, Nowak JA, González C, Iovanna J, Vaccaro MI (2007). The pancreatitis-induced vacuole membrane protein 1 triggers autophagy in mammalian cells. J Biol Chem 282, 37124–37133.

Rudinskiy M, Molinari M (2023). ER-to-lysosome-associated degradation in a nutshell: Mammalian, yeast, and plant ER-phagy as induced by misfolded proteins. FEBS Lett 597, 1928–1945.
Rusten TE, Harald S (2009). How do ESCRT proteins control autophagy? J Cell Sci 122, 2179–2183.
Ryu K-Y, Baker RT, Kopito RR (2006). Ubiquitin-specific protease 2 as a tool for quantification of total ubiquitin levels in biological specimens. Anal Biochem 353, 153–155.
Saeed B, Deligne F, Brillada C, Dünser K, Ditengou FA, Turek I, Allahham A, Grujic N, Dagdas Y, Ott T, *et al*. (2023). K63-linked ubiquitin chains are a global signal for endocytosis and contribute to selective autophagy in plants. Curr Biol 33, 1337–45.e5.
Saitoh T, Fujita N, Hayashi T, Takahara K, Satoh T, Lee H, Matsunaga K, Omori H, Noda T, Yoshimori T, Akira S (2009). Atg9a controls dsDNA-driven dynamic translocation of STING and the innate immune response. Proc Natl Acad Sci U S A 106, 20842–20846.
Sakai Y, Oku M (2024). ATG and ESCRT control multiple modes of microautophagy. FEBS Letters 598, 48–58.
Sapoń K, Mańka R, Janas T, Janas T (2023). The role of lipid rafts in vesicle formation. J Cell Sci 136, jcs260887.
Sawa-Makarska J, Baumann V, Coudevylle N, Bülow S, Nogellova V, Abert C, Schuschnig M, Graef M, Hummer G, Martens S (2020). Reconstitution of autophagosome nucleation defines Atg9 vesicles as seeds for membrane formation. Science 369, eaaz7714.
Seibenhener ML, Babu JR, Geetha T, Wong HC, Rama Krishna N, Wooten MW (2004). Sequestosome 1/p62 is a polyubiquitin chain binding protein involved in ubiquitin proteasome degradation. Mol Cell Biol 24, 8055–8068.
Shields SB, Piper RC (2011). How ubiquitin functions with ESCRTs. Traffic 12, 1306–1317.
Sicari D, Weber J, Maspero E, Polo S (2022). The NEDD4 ubiquitin E3 ligase: A snapshot view of its functional activity and regulation. Biochem Soc Trans 50, 473–485.
Sims JJ, Cohen RE (2009). Linkage-specific avidity defines the lysine 63-linked polyubiquitin-binding preference of rap80. Mol Cell 33, 775–783.
Sims JJ, Scavone F, Cooper EM, Kane LA, Youle RJ, Boeke JD, Cohen RE (2012). Polyubiquitin-sensor proteins reveal localization and linkage-type dependence of cellular ubiquitin signaling. Nat Methods 9, 303–309.
Singh S, Kumari R, Chinchwadkar S, Aher A, Matheshwaran S, Manjithaya R (2019). Exocyst subcomplex functions in autophagosome biogenesis by regulating Atg9 trafficking. J Mol Biol 431, 2821–2834.
Skowyra ML, Schlesinger PH, Naismith TV, Hanson PI (2018). Triggered recruitment of ESCRT machinery promotes endolysosomal repair. Science 360, eaar5078.
Stenmark H, Parton RG, Steele-Mortimer O, Lütcke A, Gruenberg J, Zerial M (1994). Inhibition of rab5 GTPase activity stimulates membrane fusion in endocytosis. EMBO J 13, 1287–1296.
Tamai K, Tanaka N, Nara A, Yamamoto A, Nakagawa I, Yoshimori T, Ueno Y, Shimosegawa T, Sugamura K (2007). Role of Hrs in maturation of autophagosomes in mammalian cells. Biochem Biophys Res Commun 360, 721–727.
Tan JMM, Wong ESP, Kirkpatrick DS, Pletnikova O, Ko HS, Tay S-P, Ho MWL, Troncoso JC, Gygi SP, Lee MK, Lim K-L (2008). Lysine 63-linked ubiquitination promotes the formation and autophagic clearance of protein inclusions associated with neurodegenerative diseases. Hum Mol Genet 17, 431–439.
Tsuchiya H, Burana D, Ohtake F, Arai N, Kaiho A, Komada M, Tanaka K, Saeki Y (2018). Ub-ProT reveals global length and composition of protein ubiquitylation in cells. Nat Commun 9, 1–10.
Turco E, Savova A, Gere F, Ferrari L, Romanov J, Schuschnig M, Martens S (2021). Reconstitution defines the roles of p62, NBR1 and TAX1BP1 in ubiquitin condensate formation and autophagy initiation. Nat Commun 12, 5212.
Ullrich O, Reinsch S, Urbé S, Zerial M, Parton RG (1996). Rab11 regulates recycling through the pericentriolar recycling endosome. J Cell Biol 135, 913–924.
Vale-Costa S, Etibor TA, Brás D, Sousa AL, Ferreira M, Martins GG, Mello VH, Amorim MJ (2023). ATG9A regulates the dissociation of recycling endosomes from microtubules to form liquid influenza A virus inclusions. PLoS Biol 21, e3002290.
van Wijk SJL, Fiskin E, Putyrski M, Pampaloni F, Hou J, Wild P, Kensche T, Grecco HE, Bastiaens P, Dikic I (2012). Fluorescence-based sensors to monitor localization and functions of linear and K63-linked ubiquitin chains in cells. Mol Cell 47, 797–809.
Wooten MW, Geetha T, Ramesh Babu J, Lamar Seibenhener M, Peng J, Cox N, Diaz-Meco M-T, Moscat J (2008). Essential role of sequestosome 1/p62 in regulating accumulation of Lys63-ubiquitinated proteins. J Biol Chem 283, 6783–6789.
Wurzer B, Zaffagnini G, Fracchiolla D, Turco E, Abert C, Romanov J, Martens S (2015). Oligomerization of p62 allows for selection of ubiquitinated cargo and isolation membrane during selective autophagy. Elife 4, e08941.
Xu P, Duong DM, Seyfried NT, Cheng D, Xie Y, Robert J, Rush J, Hochstrasser M, Finley D, Peng J (2009). Quantitative proteomics reveals the function of unconventional ubiquitin chains in proteasomal degradation. Cell 137, 133–145.
Yamano K, Kikuchi R, Kojima W, Hayashida R, Koyano F, Kawawaki J, Shoda T, Demizu Y, Naito M, Tanaka K, Matsuda N (2020). Critical role of mitochondrial ubiquitination and the OPTN-ATG9A axis in mitophagy. J Cell Biol 219, e201912144.
Ye Y, Rape M (2009). Building ubiquitin chains: E2 enzymes at work. Nat Rev Mol Cell Biol 10, 755–764.
Young ARJ, Chan EYW, Hu XW, Köchl R, Crawshaw SG, High S, Hailey DW, Lippincott-Schwartz J, Tooze SA (2006). Starvation and ULK1-dependent cycling of mammalian Atg9 between the TGN and endosomes. J Cell Sci 119, 3888–3900.
Zaffagnini G, Cheng S, Salzer MC, Pernaute B, Manuel Duran J, Irimia M, Schuh M, Böke E (2024). Mouse oocytes sequester aggregated proteins in degradative super-organelles. Cell 187, 1109–1126.e21.
Zaffagnini G, Savova A, Danieli A, Romanov J, Tremel S, Ebner M, Peterbauer T, Sztacho M, Trapannone R, Tarafder AK, *et al*. (2018). p62 filaments capture and present ubiquitinated cargos for autophagy. EMBO J 37, e98308.
Zavodszky E, Seaman MNJ, Moreau K, Jimenez-Sanchez M, Breusegem SY, Harbour ME, Rubinsztein DC (2014). Mutation in VPS35 associated with Parkinson's disease impairs WASH complex association and inhibits autophagy. Nat Commun 5, 3828.
Zhao YG, Chen Y, Miao G, Zhao H, Qu W, Li D, Wang Z, Liu N, Li L, Chen S, Zhang H (2017). The ER-localized transmembrane protein EPG-3/VMP1 regulates SERCA activity to control ER-isolation membrane contacts for autophagosome formation. Mol Cell 67, 974–989.e6.
Zheng YT, Shahnazari S, Brech A, Lamark T, Johansen T, Brumell JH (2009). The adaptor protein p62/SQSTM1 targets invading bacteria to the autophagy pathway. J Immunol 183, 5909–5916.
Zhou F, Wu Z, Zhao M, Murtazina R, Cai J, Zhang A, Li R, Sun D, Li W, Zhao L, *et al*. (2019). Rab5-dependent autophagosome closure by ESCRT. J Cell Biol 218, 1908–1927.